RESPONSE OF A GERMANIUM TUNNEL DIODE

TO CO_2 LASER RADIATION

Electrical G. Ribakovs, B. Eng. M. Eng.

ABSTRACT

The effects of the radiation from a CO_2 laser at $\lambda = 10.6\mu m$ on a Ge Tunnel Diode are investigated theoretically and experimentally. The perturbation of the diode tunneling current due to the intraband excitation of electrons by the incident radiation is first evaluated; then the thermal heating of the diode structure and the resulting response are investigated.

It is predicted that with a laser power of 1 watt/mm^2 and at room temperature, a S/N ratio of 4×10^4, a current responsivity of 7×10^{-7} amperes/watt, and response times of 10^{-13} sec. should be achieved by the creation of hot carriers in the conduction band of the tunnel diode. Experimentally it is found that for modulation frequencies of up to several kilohertz, a number of thermal effects appear with a range of response times from 300μsec. to 15msec., depending on the operating point on the I-V characteristic of the diode, and the magnitude of these effects dominate the faster but smaller tunneling effects.

RESPONSE OF A GE TUNNEL DIODE TO CO_2 LASER RADIATION

RESPONSE OF A GERMANIUM TUNNEL DIODE

TO CO_2 LASER RADIATION

by

Gennadijs Ribakovs, B. Eng.

A Thesis submitted to the Faculty of Graduate Studies and Research in partial fulfillment of the requirements for the degree of Master of Engineering.

Department of Electrical Engineering,

McGill University,

Montreal, Canada.

March, 1970

ABSTRACT

The effects of the radiation from a CO_2 laser at $\lambda = 10.6\ \mu m$ on a Ge Tunnel Diode are investigated theoretically and experimentally. The perturbation of the diode tunneling current due to the intraband excitation of electrons by the incident radiation is first evaluated; then the thermal heating of the diode structure and the resulting response are investigated.

It is predicted that with a laser power of 1 watt/mm^2 and at room temperature, a S/N ration of 4×10^4, a current responsivity of 7×10^{-7} amperes/watt, and response times of 10^{-13} sec. should be achieved by the creation of hot carriers in the conduction band of the tunnel diode. Experimentally it is found that for modulation frequencies of up to several kilohertz, a number of thermal effects appear with a range of response times from 300μsec. to 15msec., depending on the operating point on the I-V characteristic of the diode, and the magnitude of these effects dominate the faster but smaller tunneling effects.

ACKNOWLEDGEMENTS

The author would like to express his appreciation to Dr. A.A. Gundjian for his guidance and assistance throughout the period of research. Thanks are due to Miss Mary Ann Nikoriak for an excellent typing job.

Grateful acknowledgement is also made to the Quebec Department of Education for their financial assistance. Finally, the author would like to thank J. Foldvari for his technical assistance, and V. Krishna for his enlightening discussions.

TABLE OF CONTENTS

			Page
ABSTRACT			i
ACKNOWLEDGEMENTS			ii
TABLE OF CONTENTS			iii
LIST OF ILLUSTRATIONS			iv
CHAPTER I		Introduction	1
CHAPTER II		State of the Art of Submillimeter Detectors	4
1.0		Introduction	4
2.0		Performance of Detectors	5
3.0		Detectors	5
3.1		Point Contact Rectifiers	5
	3.1.1	Crystal Type	5
	3.1.2	MOM Tunneling Detector	6
3.2		Thermal Detectors	6
	3.2.1	General Description	6
	3.2.2	The Golay Cell	6
	3.2.3	Bolometers	7
	3.2.4	Pyroelectric	7
3.3		Photoconductors	8
	3.3.1	Intrinsic	8
	3.3.2	Extrinsic	8
3.4		Recent Advances in Detectors	9
	3.4.1	Thin Film Thermocouples	9
	3.4.2	Thin Film Bolometers	9
	3.4.3	Photon Drag Detector	9
CHAPTER III		Theoretical Analysis of the Effect of Submillimeter Radiation on Tunneling Devices	11
1.0		Introduction	11
2.0		MOS Devices	11
2.1		Physical Structure	11
2.2		Proposed Detection Mechanism	13
3.0		Tunnel Diodes	14
3.1		Introduction	14

			Page
3.2		Proposed Detection Process	17
	3.2.1	General Description	17
	3.2.2	Evaluation of the Energy Dependent Density of Excited Electrons	19
	3.2.3	Evaluation of the Proportionality Coefficient K	20
	3.2.4	Justification of the Energy Independence of K	21
	3.2.5	Probability Distribution Function for Excited Electrons	22
	3.2.6	"Quantum Efficiency"	23
	3.2.7	Definition of Δn	24
3.3		A Simple Approach to the Evaluation of the Electronic Currents Through a Tunneling Barrier Due to Excited Electrons	25
	3.3.1	Calculation of Δn (ℓ)	27
3.4		Composition of the Tunnel Diode Current	29
	3.4.1	Case (a) $h\nu < \zeta p < \zeta n$, $qV < \zeta p - h\nu$	31
	3.4.2	Case (b) $h\nu < \zeta p < \zeta n$, $qV = \zeta p$	32
	3.4.3	Case (c) $\zeta p < h\nu < \zeta n$	32
3.5		Magnitude of the Excited Tunneling Current	35
	3.5.1	Typical Parameters for a Ge Tunnel Diode	35
	3.5.2	Limiting Factors in the Response Time	37
3.6		Noise in Tunnel Diodes	38
	3.6.1	Introduction	38
	3.6.2	Thermal or Johnson Noise	38
	3.6.3	Shot Noise in Tunnel Diodes	39
	3.6.4	S/N Calculation for the Detector Circuit	41
	3.6.5	Numerical Value for S/N	44
CHAPTER IV		Heating Effects	45
1.0		Introduction	45
2.0		The Thermoelectric Effect	46
2.1		Numerical Magnitude of the Thermoelectric Effect	47
3.0		Bolometric Effect	49
3.1		Region 1, Current Due to Band-to-Band Tunneling	49
3.2		Region 2, Excess Current	50
3.3		Region 3, Thermal Current	51
3.4		Numerical Magnitude of the Bolometric Effect	51
4.0		Conclusions	52

			Page
CHAPTER V		Experimental Results	53
1.0		The Experimental Set-Up	53
1.1		The Introduction	53
1.2		The Source of Radiation	53
1.3		Modulation of the Laser Beam	53
1.4		The Tunnel Diode Detector	54
	1.4.1	The Diode Structure	54
	1.4.2	Preparation	54
1.5		Etches	54
1.6		Effect of Etching on the Tunnel Diode Characteristics	58
1.7		Electric Circuitry	59
1.8		General Experimental Procedure	66
2.0		Observed Results	66
2.1		Introduction	66
2.2		Zero Bias Signal	67
	2.2.1	Effect of Ambient Temperature	67
2.3		Signal in the Excess Current Region	68
	2.3.1	Signal at Small to Moderate Etching	68
3.0		Analysis of Results	69
3.1		Introduction	69
3.2		Discussion of the Zero Bias Signal	70
	3.2.1.	Modified Tunneling Theory	70
	3.2.1a	Component One	70
	3.2.1b	Component Two	71
	3.2.2	The Zero Bias Signal - Thermal Effects	72
3.3		Effect of Etching on the Zero Bias Signal	75
3.4		Detector Output with Bias Current	76
	3.4.1	Introduction	76
	3.4.2	Tunneling Region	76
	3.4.3	Detected Signal in the Excess Current Region	76
3.5		Ambient Temperatue Dependence of Detected Signals	77
4.0		Valley Signal Polarity Reversal at High Etching Levels	78
5.0		Conclusions	80

		Page
CHAPTER VI	Conclusion	83
APPENDIX I		85
APPENDIX II		89
REFERENCES		94

LIST OF ILLUSTRATIONS

Figure		Page
1	MOS Physical Structure	12
2	Band Diagram of MOS Structure	12
3	Tunnel Diode Band Diagram	15
4	Current-Voltage Characteristic	16
5	Effect of the Radiation on an N-Type Material	18
6	Temperature Dependence of n(E)	23
7	Junction Region	26
8a	Electron Flow Processes	26
8b	Excited Electron Concentration at $E = E_F + h\nu/2$ in Junction Region	
9	Band Diagram of Tunnel Diode	29
10	Case a: $h\nu < \zeta p < \zeta n$, $qV < \zeta p - h\nu$	33
11	Case b: $h\nu < \zeta p < \zeta n$, $qV = \zeta p$	33
12	Case c: $\zeta p < h\nu < \zeta n$	33
13	Case c: Current vs Voltage for $\zeta p < h\nu < \zeta n$	34
14	Tunnel Diode Equivalent Circuit	42
15	Detector Model	42
16	Shot Noise Current Components	43
17	Tunnel Diode Thermal Circuit	46
18	Temperature Dependence of I-V Characteristic	48
19	Diode Construction	55

Figure		Page
20	Experimental Set Up	56
21	Chopper	57
22	Junction Region of Tunnel Diode	58
23	Electric Circuitry	60
24	Zero Bias Signal at 550 Hz and Room Temperature	61
25	Excess Current Signal at 550 Hz and Room Temperature	61
26	Zero Bias Signal at 20 Hz and Room Temperature	62
27	Zero Bias Signal - Diode Etched	62
28	Zero Bias Signal near Peak Current	63
29	Zero Bias Signal at 550 Hz and Liquid Nitrogen Temperature	63
30	Zero Bias Signal at 20 Hz and Liquid Nitrogen Temperature	64
31	Valley Signal at 20 Hz	64
32	High Etching - High Current Signal	65
33	High Etching - Medium Current Signal	65
34	High Etching - Valley Current Signal	65
35	Modified Tunneling Theory	70
36	Temperature Distribution	73
37	Temperature Variation of I-V Characteristic	73
38	Surface States a) No radiation	82
	b) Radiation	82
39	Absorption Coefficient vs Radiation Frequency	82
40	Recombination Model	89
41 a	Net Excited Electron Energy Distribution	92
41 b	Net Excited Electron Density, Arbitrary Units	93

CHAPTER I

Introduction

In recent years the submillimeter band, usually taken to cover the wavelengths between 10μm and 1mm has attracted much attention. The submillimeter band bridges the gap between the optical and microwave region of the electromagnetic spectrum. It has remained relatively unexplored and unused despite the many special advantages this wavelength range could offer in applications.

The submillimeter waves are of considerable importance in fields as diverse as spectroscopic measurements, diagnostics in biological sciences, solid and liquid state studies, and in the measurement of distances using interferometer techniques; the wavelengths in this range match the tolerances sought in many machining operations in workshops. The submillimeter band is of importance to meteorologists for atmospheric studies because of the fact of the high absorption by water vapor; the latter, long a deterrent to the use of submillimeter waves for communications, is negligible in stratospheric and space applications; thus, space communication systems at these frequencies are currently being developed.

The development of electron devices performing the many conventional functions such as generation, detection, modulation, etc. of submillimeter waves is thus an active field of interest. In this work we are concerned with the analysis of the effect of a CO_2 laser radiation (λ = 10.6μm) on a Germanium tunnel diode and a discussion of the experimental response of the latter in view of the development of a detector for the submillimeter range of the electromagnetic spectrum.

A feature of this portion of the spectrum from the technological point of view, is that there are some researchers who developė techniques approaching this range from the microwave region of the spectrum, and there are those who view it from the optical region. Consequently it is not surprising that for the submillimeter region a large assortment of detectors are in use. These include point-contact rectifiers used in either video [1] or superheterodyne systems [2]; the thermal detectors such as the carbon [3], germanium [4], and superconducting bolometers [5], the Golay cell[6], the pyroelectric detector [7]; and the photoconductive detectors [5], [8].

One of the difficulties in spectroscopy in far-infared research was the lack of strong sources. One solution of this problem was to develop detectors of high responsivity. In most cases these were solid state devices which worked at liquid helium temperatures and had good responsivity but their response times were generally longer than 10^{-8} sec. With the coming of molecular lasers in the submillimeter band, such as the CO_2 (λ = 10.6μm), H_2O (λ = 28μm), SO_2(λ = 215μm), HCN (λ = 337μm), and other lasers, responsivity could give way to speed.

Quantum mechanical tunneling [9], being one of the fastest physical phenomena known and also being largely temperature independent, it was quite natural to attempt to utilize the tunneling principle to develope an extremely fast far-infrared detector at room temperature. Two devices whose current-voltage characteristics are governed by the tunneling mechanism are MOS structures (with an oxide thickness less than 100^{o}A) [10], and the Esaki or tunnel diode [11] ; the response of the latter subjected to radiation from a CO_2 laser will now be described and discussed in detail.

CHAPTER II

State of the Art of Submillimeter Detectors

II 1.0 Introduction

The following is one possible classification of millimeter to infrared detectors according to their physical mechanism of operation:

a) Point Contact Detectors

1. Crystal
2. Metal Oxide Metal (MOM)

b) Thermal Detectors

1. Pneumatic (Golay cell)
2. Bolometers
3. Pyroelectric

c) Photoconductors

1. Intrinsic
2. Extrinsic

II. 2.0 The Performance of Detectors

The performance of the detectors will be described by a consideration of three quantities [8], [43] :

1) the responsivity $R_V = \Delta V/\Delta W$, in volts/watt, or $R_I = \Delta I/\Delta W$ in amperes/watt, where ΔV , ΔI are the output voltage and current respectively produced by a change ΔW in the input signal power;
2) the noise equivalent power NEP, in watts/Hz$^{1/2}$, which is the signal power required to give an output voltage equal to the noise output from the detecting system with unit bandwidth;
3) the response time τ, which is a measure of the time necessary for the detector to react to a sufficiently rapid change in the incident power flux.

II. 3.0 Detectors

II. 3.1 Point Contact Rectifiers

II. 3.1.1 Crystal Type

These diodes are fabricated by applying a metallic pressure conduct to a semiconductor crystal. In these devices one uses the non-linear components in the Taylor series expansion of the current density in order to detect, modulate and mix electromagnetic radiation. While point contact diodes have been used as video detectors to wavelengths as short as 0.5 mm. [1], their performance starts falling below about 1 cm. due to the shunting effect of the contact capacity. Noise equivalent powers NEP of 10^{-11} watts/Hz$^{1/2}$ at 2mm wavelength using germanium rectifiers with a video receiver [2] have been obtained.

II. 3.1.2 MOM Tunneling Detector

A recent development, the metal-oxide-metal (MOM) point contact detector [12] appears to be the fastest response, broadest frequency coverage device thus far discovered. The oxide is the natural oxide that is present on the surface of any metal. This device has detected signals from DC to 10μ wavelength and its response time is less than 10^{-13}sec. A typical diode has a responsivity of 300-1000 volts/watts and a NEP of 10^{-9} to 10^{-10} watts/Hz$^{1/2}$ at room temperature.

The MOM diode has been employed in the same configuration as the run-in microwave semiconductor inguide diode. The non-linear I-V characteristic of the diode, explained by the independent-electron theory of tunneling, is used to detect the radiation.

II. 3.2. Thermal detectors

II. 3.2.1 General Description

Thermal detectors include bolometers, Golay cell, and the pyroelectric detector. Two general characteristics of thermal detectors are that their performance is independent of wavelength, and that their time constants are relatively long. The exception to the latter fact is the pyroelectric detectors which can have response times in the order of tens of nanoseconds.

II. 3.2.2 The Golay Cell

This is a pneumatic detector [6] . The absorbed ratiation heats up the gas enclosed in a small cavity, one of whose walls is a thin flexible membrane. This wall is distorted by changes in the pressure of the gas when heated by the radiation. The outside of the membrane forms a mirror which deflects a beam of light shining onto a photocell which in turn produces an electric signal. Manufacturers of Golay cells claim NEP of about 10^{-10} watts/Hz$^{1/2}$ with time constants of about 15msec at room temperature.

II. 3.2.3 Bolometers

A bolometer is constructed from a material with a high temperature coefficient of resistance. It is arranged so that the absorption of radiation causes its temperature to rise, hence producing a change in resistance which can be observed by a suitable bridge or amplifier circuit. In this type of detector, usually made from carbon or germanium, the energy is absorbed by the free carriers of an impurity or of the conduction band itself. The photoresponse is over the wavelength of 20-1000μm, with response times of about 100μsec, and NEP's of 10^{-13} W/Hz$^{1/2}$. Cooling a bolometer will increase its ultimate sensitivity by reducing thermal fluctuations. These detectors are usually cooled to approximately liquid helium temperatures [8].

II. 3.2.4 Pyroelectric Detectors

Pyroelectric detectors are thermal detectors capable of operating at room temperature and responding to high frequencies. Consequently they may be used to detect any radiation which causes a change in the detector temperature (x-rays to microwaves). However, they are different from other thermal detectors in that the current responsivity is frequency independent, for frequencies above the reciprocal thermal relaxation time of the detector system (typically 1 to 0.1/secs). These devices have been used to detect CO_2, H_2O and HCN laser pulses with response times as short as a few n-secs. However, as with many other detectors this bandwidth can only be obtained at the expense of voltage responsivity, and signal to noise ratio since they have to be loaded with a small resistor to avoid RC attenuation of the signal in the detector circuit.

II. 3.3 Photoconductive detectors

The long wavelength threshold of these detectors is determined by the minimum photon energy necessary to excite an electron from one energy level to a second.

II. 3.3.1 Intrinsic photoconductors have narrow energy gaps between their valence and conduction bands enabling far infrared radiation to create electron hole pairs which then cause a conductivity change in the material. Two such intrinsic photoconductors are Mercury Cadium Telluride and Indium Antimonide.

II. 3.3.2 Extrinsic photoconductors utilize photoexcitations from shallow donors or acceptors in semiconductors. The most common material in use today is germanium doped with either gold, antimony (both donors) or Indium (acceptor). These detectors exhibit photoresponse over the wavelength region 50 - 120 μm and their responsetime is less than 1 μsec with typical NEP of 10^{-11} watts/$Hz^{1/2}$. Also the photoconductors are cooled to reduce thermal excitation of electrons and thus increase their sensitivities.

II. 3.4 Recent Advances in Detectors

The following room temperature detectors have appeared in the literature after the preparation of this work.

II. 3.4.1 Thin Film Thermocouples

A thin film thermocouple detector, suitable for use with lasers operating in the middle and far-infrared region of the spectrum, has been developed. It utilizes a $1000A^{o}$-thick film of bismuth or silver on beryllium oxide substrates [39]. Measured response times are approximately 10^{-7}sec. The responsivity is found to be 4μ V/W and the noise equivalent power is of the order of 10^{-7} $W/Hz^{1/2}$.

II. 3.4.2 Thin Film Bolometers

It has been reported [40] that thin film bolometers have been proven useful as room temperature laboratory detectors for pulsed infrared and far-infrared lasers. These detectors are fabricated by the deposition of thin films of bismuth or nickel on beryllium oxide or silicon dioxide substrates. The measured response time is less than 15 nsec, the NEP is found to be less than 10^{-6} $W/Hz^{1/2}$, and the responsivity is from 10^{-4} to 10^{-3} V/W.

II. 3.4.3 The Photon Drag Detector.

The transfer of momentum from a photon stream to free electrons and holes in germanium has been studied [41], [42]. It is shown that a Q-switched CO_2 laser can transfer sufficient momentum to produce a longitudinal emf or current in a germanium rod. This effect provides a useful, high speed ($\approx 10^{-13}$ sec) detector, with a responsivity of approximately 10^{-7} V/W, operating at room temperature.

CHAPTER III

Theoretical Analysis of the Effect of Submillimeter Radiation on Tunneling Devices

III. 1.0 Introduction

Two basic types of tunnel barrier devices are considered for the detection of submillimeter radiation. They are the metal-oxide-semiconductor MOS structure [13] and the tunnel diode [14].

Quantum mechanical tunneling describes the situation where a particle passes through a narrow potential barrier instead of surmounting it, without change in energy. Both of the above mentioned devices are characterized by having low enough barrier heights and thickness in order to allow an appreciable tunneling probability to exist.

III. 2.0 MOS Devices

III. 2.1 Physical Structure

Figure 1 shows the MOS structure which consists of an oxide grown on a single crystal semiconductor wafer of known doping concentration. Figure 2 represents the energy diagram for an MOS structure, where the oxide layer acts a a rectangular potential barrier between the metal and semiconductor layers. ψ_m and ψ_s , called the work functions of the metal and semiconductor respectively, are of the order of 3 to 4 electron volts. When the oxide layer thickness is less than about 100A^{o} an appreciable tunneling probability exists for electrons across the rectangular energy barrier.

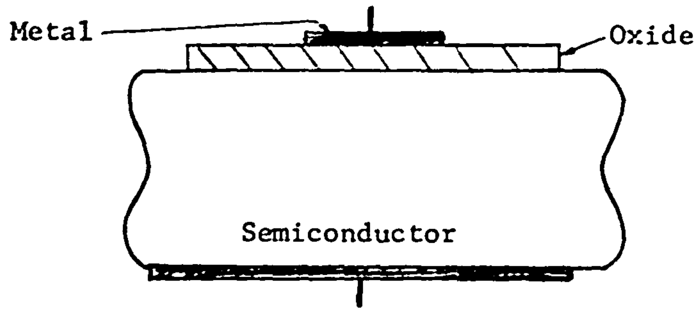

Figure 1 MOS Physical Structure

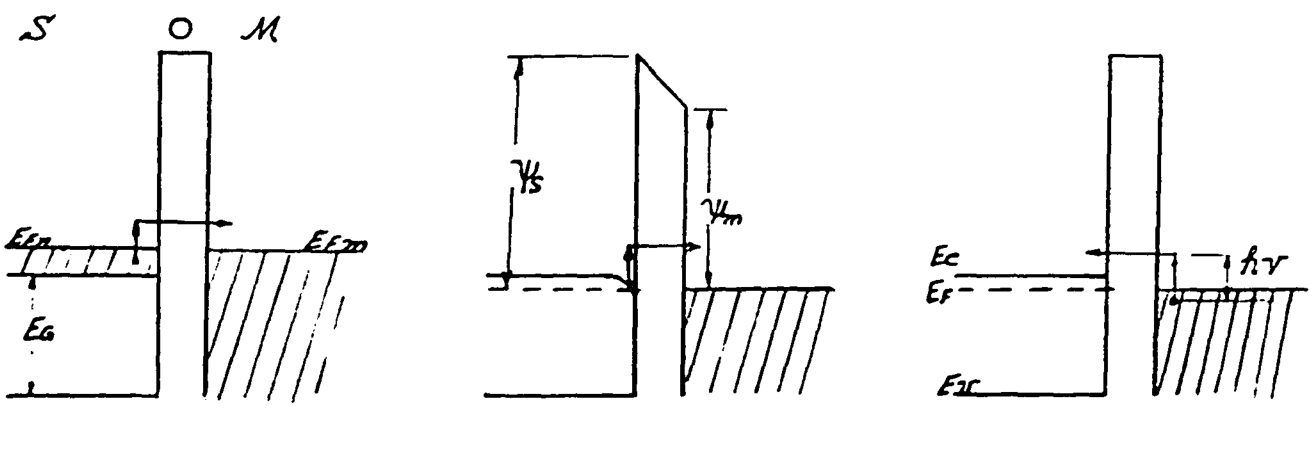

Figure 2

Band Diagram of MOS Structure

III. 2.2 Proposed Detection Mechanism

Three possible ways of using MOS structures as far-infrared detectors are shown in Figure 2.

Case (a): This is the case shown in figure 2a where the semiconductor is degenerate in order to allow a substantial absorption of radiation. If radiation, incident on a semiconductor is absorbed by free carriers (in the degenerate conduction band in this case) their energy will be increased above the equilibrium value by hv (where h is Plank's constant and v the radiation frequency) resulting in a change in the tunneling probability and correspondingly a change in current. In this configuration, radiation is absorbed along the whole length of the radiation beam in the semiconductor region. The amount of electrons excited near the barrier, which are, as shown later, to be the ones mainly responsible for the tunneling current, is reduced because of the large amount of absorption in the bulk of the semiconductor.

Case (b): Clearly an improvement on the preceeding scheme is when a degenerate semiconductor is created only near the barrier region, figure 2b. An n-type semiconductor with a metal having a much lower work function is used. If the difference in work functions is large enough, the conduction band edge of the semiconductor will bend down below the fermi-energy producing a strong accumulation region near the barrier [16]. This bending of the bands can be further increased by applying an appropriate bias. Thus most of the absorption will occur only near the barrier. In this case however, it can be shown that the total amount of absorbed power within the relatively narrow accumulation region is very small thus reducing the efficiency of the device.

Case (c): In the third case, figure 2c, a high resistivity semiconductor is used which has very few free carriers to absorb any radiation, thus the semiconductor is practically transparent to sub band gap radiation. The radiation passes through the semiconductor and barrier and is strongly absorbed by the metal at the metal-oxide interface region because of the large number of free electrons in the metal. Once these electrons have been excited to a higher energy level, they will tunnel through the barrier into the semiconductor as shown in figure 2c.

Since the fabrication of tunneling MOS structures had to be first perfected before they could be used for the proposed detection scheme, therefore it was decided at this point to use, for the rest of this work, an already well known tunneling structure such as the tunnel diode for the purpose of investigating its response to far-infrared radiation.

III. 3.0. Tunnel Diodes

III. 3.1 Introduction

In 1957 it was discovered by L. Esaki that very heavily doped p-n junction diodes with impurity concentrations in the order of 10^{19} cm^3, exhibit a peak current at low voltages in the forward part of the current-voltage characteristic. This effect was successfully explained by the quantum-mechanical tunneling of electrons through the p-n junction potential barrier.

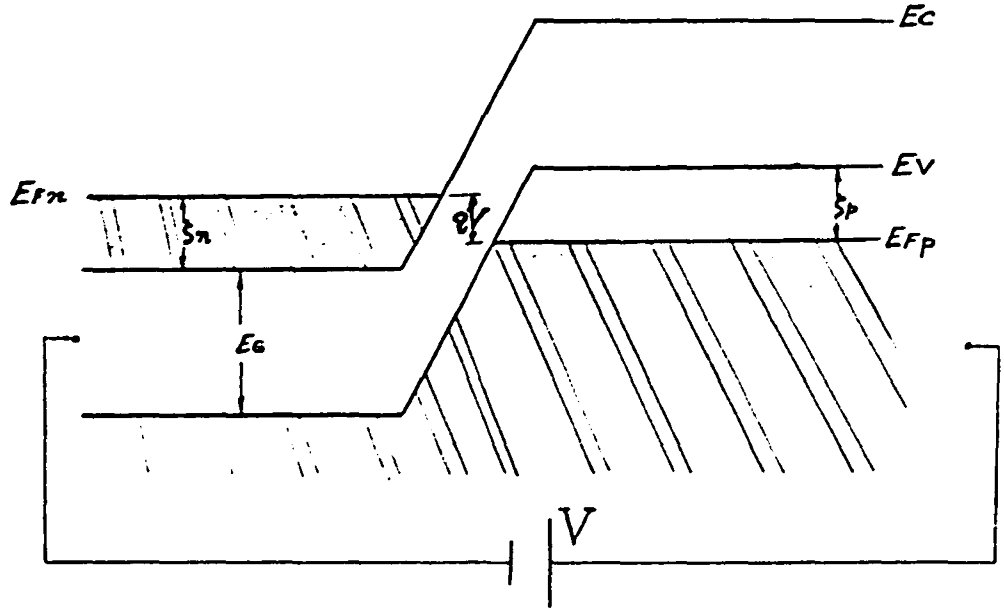

Figure 3 Tunnel Diode Band Diagram

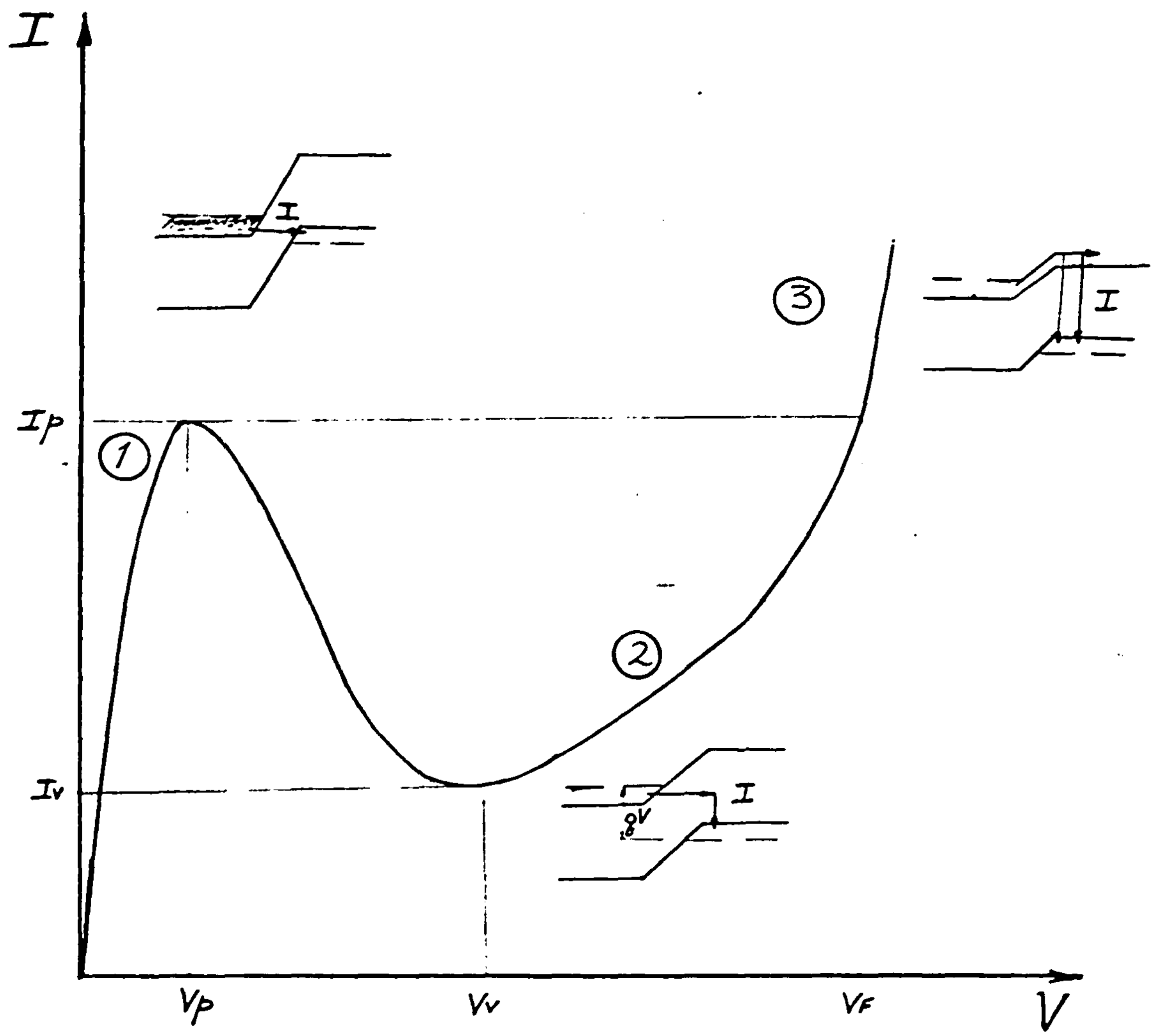

Figure 4 Current-voltage characteristic of a tunnel diode. Inserts show the relative positions of the bands and the paths of electron flow for three principle components of current.

The current-voltage characteristic of a tunnel diode is explained with the energy band diagram of the device shown in figure 3. The current-voltage characteristics of a tunnel diode, figure 4, consists of three regions:

1) In the reverse and low forward bias region, the current is the result of quantum mechanical band to band tunneling.
2) The current at intermediate forward bias is the excess current which is attributed to tunneling via localized states in the energy gap.
3) The current at high forward bias values is the usual p-n junction thermal current.

III. 3.2 Proposed Detection Process

III. 3.2.1 General Description

Since the semiconductor of an Esaki diode is made of degenerate material, there are many free carriers available to absorb the far infrared radiation (see Appendix I). It is assumed that when an electron absorbs a photon its energy will be increased by an amount equal to the photon energy. These higher energy electrons, called "excited electrons" will cause a current change in the device which will be used for the detection of the incident radiation. The remainder of this paper will deal with the theoretical study and experimental results of a tunnel diode's response to far-infrared radiation.

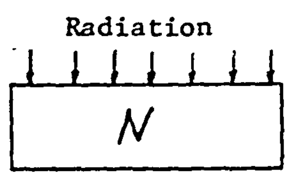

a) Illumination of N-type Material

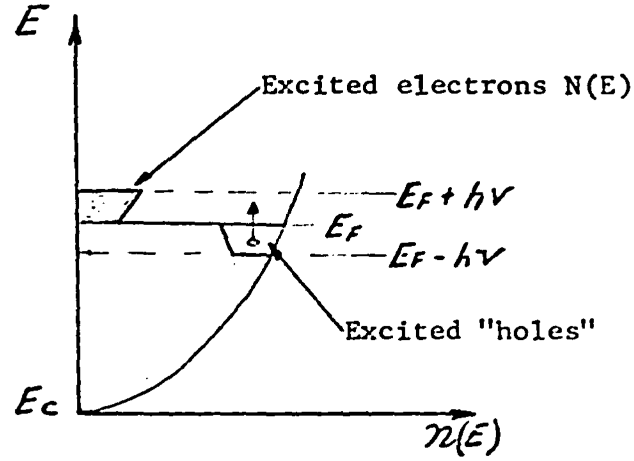

b) Perturbation of the energy distribution of electrons at T = 0° K

Figure 5

Effect of the Radiation on an N-type Material

III. 3.2.2 Evaluation of the energy dependent density of radiation excited electrons

Let N(E) be the density of electrons excited to an energy level E, and n(E) be the density of unexcited or equilibrium electrons at energy E, i.e.

$$n(E) = g(E)\, f(E) \tag{1}$$

where

g(E) is the density of allowed states at an energy level E

and

f(E) is the fermi distribution function.

Suppose that an n-type semiconductor is uniformly illuminated along its whole length, as in Figure 5a, with radiation having an energy hv per photon. If this radiation is absorbed by the free carriers, it is assumed that the density N(E) of electrons excited to an energy E is proportional to the density of unoccupied energy states at E and the number of occupied states at (E-hv).

Then the density of electrons excited to an energy E is

$$N(E) = K'\, g(E)[1 - f(E)]\, g(E-hv)\, f(E-hv)$$

where K' is a proportionality coefficient under the condition that the integral of N(E) over the whole conduction band equals Δn defined as the total number of excited electrons per unit volume, i.e.

$$\Delta n = \int_{E_c}^{\infty} N(E)dE = \int_{E_c}^{\infty} K'\, g(E)[1-f(E)]g(E-hv)f(E-hv)dE \tag{2}$$

In degenerate semiconductors

$$g(E) \;\alpha\; E^{1/2} \text{ assuming band parabolicity,}$$

$$\therefore \quad N(E) = K\sqrt{E(E-hv)}\,[1 - f(E)]\,f(E - hv) \tag{3}$$

Let $N_{net}(E)$ be the <u>net</u> number of excited electrons at an energy E which is equal to N(E) the number of electrons excited <u>to</u> E minus N(E + hv) the number of electrons excited <u>from</u> E , i.e.

$$N_{net}(E) = N(E) - N(E + hv) \tag{4}$$

This expression is valid over the whole conduction band and at all temperatures.

At $T = 0^o$ K and if $hv < E_F$, expanding $\sqrt{E(E - hv)}$ into a Taylor's series and retaining the first two terms only, a simplified expression is obtained:

$$\begin{aligned} N_{net}(E) &\approx K(E - hv/2) && \text{for} \quad E_F < E < E_F + hv \\ N_{net}(E) &\approx -K(E + hv/2) && \text{for} \quad E_F - hv < E < E_F \\ N_{net}(E) &\approx 0 && \text{elsewhere.} \end{aligned} \tag{5}$$

In the energy range $E_F - hv < E < E_F$, the negative value for $N_{net}(E)$ denotes an absence of electrons, since the elctrons which have been excited to higher energy levels have been extracted from energy levels in that range, see Figure 5b.

III. 3.2.3 <u>Evaluation of the proportionality coefficient K at $T = 0^oK$</u>

Examining equations (4) and (3) at $T = 0^oK$ it is readily seen that $N(E) = N_{net}(E)$ for $E > E_F$. Thus substituting equation (5) into equation (2) we get

$$\int_{E_F}^{E_F + h\nu} K(E - \frac{h\nu}{2})dE = \Delta n \qquad (6)$$

K can be assumed to be independent of energy as it will be shown in section 3.2.4. Thus integrating equation (6) and solving for K ,

$$K = \frac{\Delta n}{E_F h\nu} \qquad (7)$$

Now putting (7) into (5)

$$N(E) = \frac{\Delta n}{E_F h\nu}\left(E - \frac{h\nu}{2} \right) \quad \text{when} \quad E_F < E < E_F + h\nu \qquad (8)$$

The zero-order approximation would give N(E) a constant if $h\nu \ll E_F$, i.e. $E - h\nu/2 \approx E_F$. Then

$$N = \frac{\Delta n}{h\nu} \qquad (9)$$

III. 3.2.4 Justification of Energy Independence of K

For the evaluation of N(E), the assumption that the proportionality factor K was independent of E was used. This factor implicitly involves transition probabilities between two states with momentum vectors k and k' at energy levels E_k and $E_{k'}$. One of the forms for writing the transition probability $P_{kk'}$ is [17]:

$$P_{kk'} = \text{const.}\ W_{kk'}(k-k')^2 \ \delta(E_{k'} - E_k - h\nu) \qquad (10)$$

where $W_{kk'}$ is in the form of the usual probability per unit time found when scattering between states at the same energy is considered;

$E_{k'}$ and E_k are the final and initial energy states;

The Kronecker Delta $\delta(x) = \begin{cases} 1 \text{ iff } x = 0 \\ 0 \text{ otherwise} \end{cases}$.

Thus since the transition probability is independent of E and depends only on the difference between initial and final states denoted by their momentum vectors k and k' , the assumption that K is independent of energy is valid.

III. 3.2.5 Probability Distribution Function for Excited Electrons

We can assign the excited electrons a probability distribution function $F_1(E)$ defined as the ratio of occupied states N(E) to available states g(E) at an energy E,

$$F_1(E) = N(E)/g(E) \; . \qquad (11)$$

This quantity, as will be shown in the next section, is important in determining the magnitude of the incremental tunneling current due to the excitation of electrons. The magnitude of $F_1(E)$ can be found easily in terms of known quantities if the following facts are considered. Since the energies E in question do not deviate much from E_F i.e. $h\nu \ll E_F$, it can be assumed that $g(E) \approx g(E_F)$ for all E.

Now the total number of free carriers n in the conduction band equals the donor doping density N_D for a degenerate material.

$$N_D = n = \int g(E)\, f(E)\, dE$$

but

$$g(E) = \frac{4\pi(2m^*)^{3/2}}{h^3} E^{1/2} \qquad (12)$$

at $T = 0$, $f(E) = 1$

$$N_D = \int_0^{E_F} \frac{4\pi(2m^*)^{3/2}}{h^3} E^{1/2}\, dE$$

$$= {}^2/_3\, E_F \left[\frac{4\pi(2m^*)^{3/2}}{h^3} E_F^{1/2}\right]$$

$$= {}^{2}/_{3}\, E_F\, g(E_F)$$

$$\therefore \quad g(E_F) = {}^{3}/_{2}\, \frac{N_D}{E_F} \tag{13}$$

$$\therefore \quad F_1(E) = \frac{N(E)}{g(E_F)} = \frac{\Delta n\, [E - {}^{hv}/_{2}]}{E_F\, hv} \cdot \frac{2}{3}\, \frac{E_F}{N_D}$$

$$F_1 = \frac{2}{3}\, \frac{\Delta n\, (E - {}^{hv}/_{2})}{N_D\, hv} \tag{14}$$

and if $E - {}^{hv}/_{2} \approx E_F$ for all E

$$\text{then} \quad F_1 = \frac{2}{3}\, \frac{\Delta n}{N_D}\, \frac{E_F}{hv} \tag{15}$$

Thus the ratio of Δn to N_D will be an important quantity in determining the tunnel current due to excited electrons.

III. 3.2.6 "Quantum Efficiency"

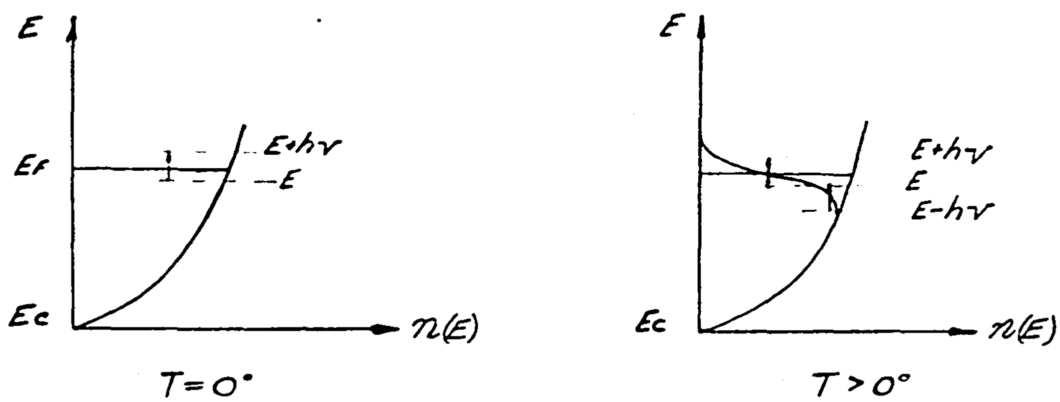

Figure 6 Temperature Dependence of n(E)

At T = 0, every electron that absorbs a photon at an energy E causes an absence of an electron at E (refer fig. 6a) and an excited electron at

E + hv. This vacancy at E, caused by the excitation of an electron, can be regarded as the creation of an "excited hole" at energy E. On the other hand, no other electrons from E-hv can be excited to energy E. This is due to the unavailability of states at E as is illustrated by the factor [1-f(E)] in equation (3), since f(E) = 1 for all energies below the fermi level if the presence of "excited holes" are neglected. Thus one can say that for every photon absorbed an excited electron and hole exists and in this sense the quantum efficiency is unity.

At finite temperatures there are already both empty and occupied states at certain energies E, below and above E_F, due to the thermal tails on the fermi distribution function as shown in equation (1). Therefore a "hole" can be created at the energy E by an electron going to E + hv as given by the term N(E+hv) in equation (4), but also an electron can be excited to the level E from the lower energy E - hv . Thus the effect is that for one excited electron at E+hv, on the average more than one photon has been absorbed. Therefore the effective quantum efficiency will be reduced at finite temperatures.

From equation (4), various excited electron concentrations have been computed on a computer and are plotted in Figures 41a and 41b. The distributions depend strongly on the temperature and hv.

III. 3.2.7 Definition of Δn

The parameter Δn was defined as the total number of electrons per unit volume that are excited by the absorption of radiation. Generally

$$\Delta n = G\tau$$

where G is the rate at which excited electrons are generated, and τ is the electron energy relaxation time

$$G = \frac{P(x)\,\gamma}{hv}$$

where

P is the absorbed power per unit volume at a point x ,

$h\nu$ is the energy per photon,

γ is the quantum efficiency.

The quantity $P/h\nu$ is clearly the number of photons/vol-sec. that are absorbed. If $\Pi(A,x)$ is the total power of the beam of cross section A at a point x, the power volume density is then

$$P(x) = -\frac{\partial}{\partial x}\left[\frac{\partial \Pi(A,x)}{\partial A}\right] = -\frac{\partial}{\partial x} I(x) .$$

where I(x) is the power per unit area.

Since the power decays exponentially as it is absorbed in the material, i.e. ;

$$I(x) = I_o e^{-\alpha x}$$

where I_o is the incident power per unit area,

α is the absorption constant.

Then

$$P(x) = \alpha I_o e^{-\alpha x}$$

and

$$n(x) = \frac{\alpha \tau I_o e^{-\alpha x}}{h\nu} \gamma \tag{16}$$

III. 3.3 A Simple Approach to the Evaluation of the Electronic Currents Through a Tunneling Barrier Due to Excited Electrons

Suppose the n-side of a tunnel diode (see Fig. 7)is uniformly illuminated with photons of energy $h\nu$ at the rate of G photons per sec. Assuming that this energy is absorbed, with a quantum efficiency of unity, by the free carriers in the degenerate conduction band, it causes a shift in the concentration distribution about the fermi-level as indicated in the previous section.

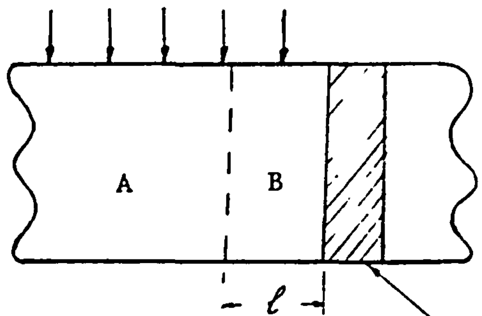

Figure 7 Junction Region

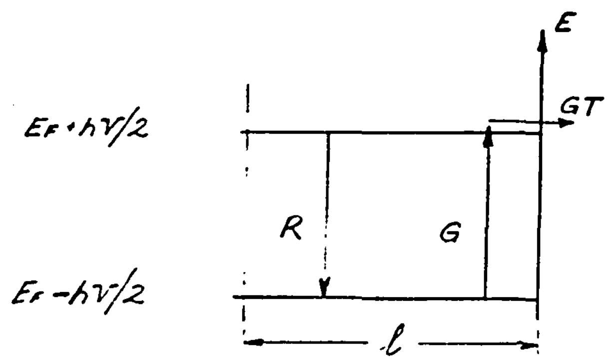

Figure 8a Electron Flow Processes

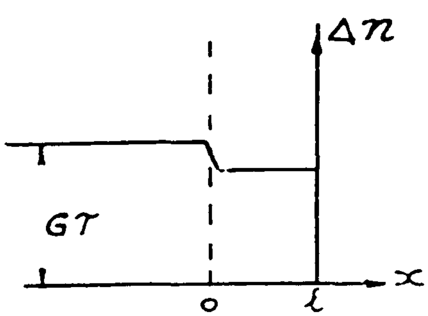

Figure 8b

Excited Electron Concentration at $E = E_F + h\nu/2$ in Junction Region

The n-region can be divided into two parts; region A, located within a mean free path length "ℓ" from the tunneling barrier; and region B, the remainder of the bulk region.

Within the mean free path region and through the barrier, a tunneling current exists consisting of two components:

1) The first component arises from electrons within the mean free path that are not affected by scattering and relaxation processes and tunnel directly after being excited. The number of these electrons per sec. and per unit junction area in the mean free path " ℓ " is given by ℓG ; clearly only ℓGT, of these electrons tunnel through the barrier where T is the probability of tunneling through the energy barrier at the junction.

2) The second component of current originates from the density of steady state excited electrons, $\Delta n(\ell)$, at the barrier which strikes the barrier with a velocity v_x. Of these $\Delta n(\ell)$ excited electrons, only $\Delta n(\ell)T$ are able to tunnel. Therefore at the barrier the total excited current J_{ex} is the sum of these two current components.

$$J_{ex} = -q \left[\ell GT + v_x \Delta n(\ell)T \right] \tag{17}$$

III. 3.3.1 Calculation of $\Delta n\ (\ell)$

Assume for simplicity that $0 < x < \ell$

$\Delta n = \Delta n\ (\ell)$ i.e. a constant in the mean free path region.

The detailed continuity equation in this region can be written as follows:

$$\frac{\partial(\Delta n)}{\partial t} = G - \frac{\Delta n(\ell)}{\tau} - \nabla . J \tag{18}$$

where

$\frac{\Delta n\,(\ell)}{\tau}$ is the net rate of recombination,

$\nabla . J$-is the rate of change of the current/unit length in the mean free path region and is given by GT.

$$\therefore \quad \frac{\partial(\Delta n)}{\partial t} = (1 - T)G - \frac{\Delta n\,(\ell)}{\tau} \tag{19}$$

From this equation it can be seen that the effective generation rate in this region has been reduced since TG electrons per unit volume have left directly without partaking in the relaxation processes.

At steady state $\frac{\partial(\Delta n)}{\partial t} = 0$.

$$\therefore \quad \Delta n(\ell) = (1 - T)G\tau \tag{20}$$

Figure 8b shows the concentration profile of $\Delta n\,(x)$ in the two regions. In the bulk region where there is no tunneling electrons, the number of excited electrons is given by the usual expression $G\tau$.

The total excited current can now be written as:

$$J_{ex} = -q \left[\ell G T + v_x (1 - T)\, G \tau T \right] \tag{21}$$

If $\ell \simeq v_x \tau$ and $T << 1$, then

$$\begin{aligned} J_{ex} &\approx -2qv_x \tau GT \\ &\approx -2q\ell GT \end{aligned} \tag{22}$$

This is a simplified expression for the excited tunnel current in one direction only, i.e. it neglects the presence of "excited holes". It also treats all the excited electrons as if they were concentrated at one energy level. Nevertheless, it is a useful expression in determining the order of magnitude for the excited current and it also includes most of the important parameters determining this current. A more rigourous derivation of the tunnel current taking into account energy dependences is given in the next section.

III. 3.4 Composition of the Tunnel Diode Current

For a tunnel diode as shown in Figure 9, current or the number of electrons striking the junction per sec. per unit area of junction is given by the product of the electron density of occupied states in a band and the velocity of these electrons in the appropriate direction. Thus the incident current from the left hand side in Figure 9 is calculated as:

$$d\,Ji = -qv_x \frac{1}{4\pi^3} f_1(E_1)\, dk_x\, dk_y\, dk_z$$

where k_i - momentum vector in the direction i,

$\frac{1}{4\pi^3}$ - density of available states in k-space.

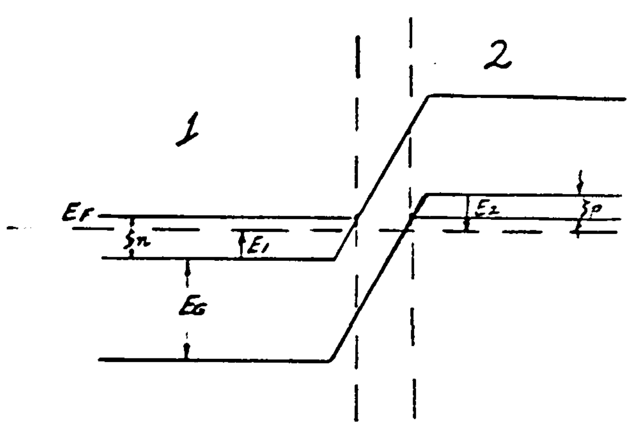

Figure 9 Band Diagram of Tunnel Diode

By definition of the transmission coefficient T, the tunnel current dJt through the barrier into the energy band on the left hand side is related to dJi through T . dJt must be reduced by $[1 - f_2(E_2)]$ for a partially filled band where E_1 and E_2 in the distribution functions represent the initial and final energy states as shown in Figure 9 . Therefore the current due to electrons going from the conduction band of region 1 to the valence band of region 2, is:

$$Jt(c \rightarrow v) = \iint -q \frac{4\pi}{h^3} \; T \; f_1(E_1) \; [1-f_2(E_2)] \; m^* \, d\,E_x \, d\,E_\perp$$

where $E_\perp = \dfrac{\hbar(k_y{}^2 + k_z{}^2)}{2m^*}$; $E_x = \dfrac{\hbar \; k_y 2}{2m^*}$; m^* is the effective mass of an electron.

Subtracting the current from the opposite direction $Jt(v \rightarrow c)$, the total tunneling current is:

$$Jt = \iint q \frac{4\pi}{h^3} \; T \; [f_1(E_1)-f_2(E_2)] m^* \, d\,E_x \, dE_\perp \tag{23}$$

The transmission probability given by Kane [18] for direct tunneling, i.e. for tunneling between the conduction and valence band extrema at the same point in k-space is:

$$T = \frac{\pi^2}{9} \exp \frac{-\pi \; m^{*1/2} \; E_G{}^{3/2}}{2\sqrt{2} \;\; h \; q \; \mathcal{E}} \quad \exp \frac{-\sqrt{2} \; m^{*1/2} \; E_\perp \, E_G{}^{1/2}}{h \; q \; \mathcal{E}} \tag{24}$$

where $\mathcal{E}$ is the electric field in the junction area.

Germanium being an indirect gap material, it would be expected that T should be modified extensively for this case, however, it has beenobserved that the transition in Ge tunnel diodes, with P or As doping, occur without phonon assistance [38]. The momentum selection rules appear to have changed due to the heavy impurity concentrations. Consequently, it is found [24] reasonable to apply Kane's calculation for direct transition as given in equation (24) to the case of Ge diodes

$$\text{Let} \quad \overline{E_\perp} = \frac{2h \, q \, \mathcal{E}}{\pi \; m^{*1/2} \; E_G{}^{1/2}} \tag{25}$$

then

$$Jt = \frac{9m^*}{18\hbar^3} \exp\left(\frac{-E_G}{\overline{E_\perp}}\right) \iint \; [f_1(E)-f_2(E)] \exp\left(\frac{-2E_\perp}{\overline{E_\perp}}\right) dE_\perp dE \tag{26}$$

To evaluate the tunneling current due to the excited electrons, equation (26) is rewritten in the following form by grouping all the constants into A'.

$$Jt = A' \iint \left[f_1(E_1) - f_2(E_2) \right] \exp\left(\frac{-2E_\perp}{\overline{E}_\perp} \right) dE_\perp \, dE \; .$$

The limits of $E_\perp$ are $0 \leq E_\perp \leq E_1$

$0 \leq E_\perp \leq E_2$

since the total energy $E = E_x + E_\perp$ and the momentum in the transverse direction must be conserved.

$\therefore$ Let Es be the smaller of E_1 and E_2 .

Now integrating once wrt $dE_\perp$

$$Jt = A \int \left[f_1(E_1) - f_2(E_2) \right] \left[1 - \exp\left(\frac{-2Es}{\overline{E}_\perp} \right) \right] dE \qquad (27)$$

where $A = \dfrac{em^* \overline{E}_\perp}{36\hbar^3} \exp\left(\dfrac{-E_G}{2\overline{E}_\perp} \right)$.

In the calculations to follow, only currents due to excited electrons and holes are considered. The normal D-C components of current are neglected. The distribution functions f_1 and f_2 for excited carriers are:

$f_2 = 0$ since no excited carriers are assumed to be in the valance band

and $f_1 = F_1$ when $E_{F_n} < E < E_{F_n} + hv$

where F_1 is the distribution function of excited electrons, and E_{F_n} is the fermi level in the conduction band,

similarly $f_1 = -F_1$ when $\left(E_{F_n} - hv\right) < E_1 < E_{F_n}$

where $-F_1$ indicates the presence of excited holes in this energy range.

III. 3.4.1

Case (a) corresponds to the conditions that the amount of degeneracy ξp in the p-side of the diode is less than the amount of degeneracy ξn in the n-side; the radiation energy hv is less than p; and the applied bias qV is less than the quantity ξp-hv . Refer to Figure 10.

Substituting the appropriate distribution function for excited carriers into equation (27),

$$Jt = A \int_{-hv}^{o} - F_1(E_1)\left[1 - \exp - 2\left(\frac{\zeta p - qV - E}{\bar{E}_\perp}\right)\right] dE$$

$$+ A \int_{o}^{hv} F_1(E_1)\left[1 - \exp - 2\left(\frac{\zeta p - qV - E}{\bar{E}_\perp}\right)\right] dE$$

For simplicity we use the zero-order approximation for $F_1(E)$ = const. given as in equation (15). Then

$$Jt = 2AF_1 \bar{E}_\perp \exp - \frac{2(\zeta p - qV)}{\bar{E}_\perp} \sinh^2 \frac{hv}{\bar{E}_\perp} \quad . \tag{28}$$

III. 3.4.2

Case (b): In this case the conditions are that $qV = \zeta p$, $\zeta n > \zeta p$, and $hv < \zeta p$.

Referring to Figure 11, the tunneling current is expressed as:

$$Jt = -A F_1 \int_{o}^{hv}\left[1 - \exp - \frac{2(hv - E)}{\bar{E}_\perp}\right] dE$$

$$= -A F_1 \left[hv - \frac{\bar{E}_\perp}{2} \left(1 - \exp \left(\frac{-2hv}{\bar{E}_\perp}\right)\right)\right] \tag{29}$$

This expression can be further simplified if it is assumed that $hv < \frac{\bar{E}_\perp}{2} \simeq \frac{\zeta p}{2}$ i.e. for radiation of wavelength $\infty > \lambda > 100\mu m$. Then

$$Jt \simeq - A F_1 \frac{(hv)^2}{\bar{E}_\perp} \tag{30}$$

III. 3.4.3

Case (c): The previous calculations have dealt with the excited tunneling current when the condition that $hv < \zeta p$ is satisfied. Now consider the condition when $hv > \zeta p$ but still less than ζn in order that the condition $F_1 =$ const. is still ensured. Refer to Figure 12.

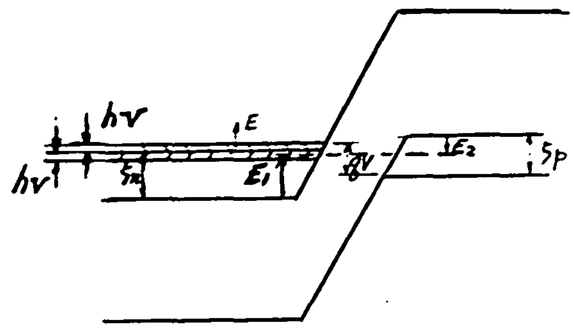

Figure 10 Case a) hv < ζp < ζn , qV < ζp - hv

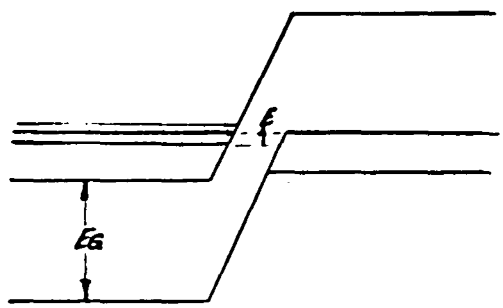

Figure 11 Case b) hv < ζp < ζn , qV = ζp

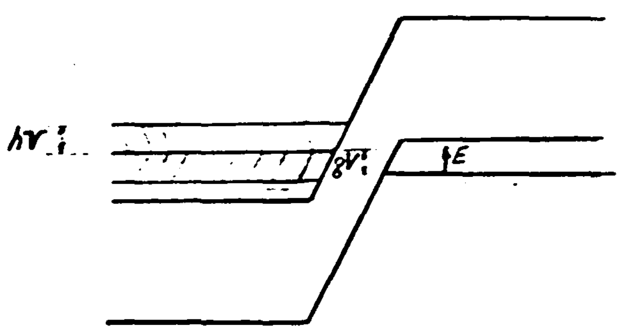

Figure 12 Case c) ζp < hv < ζn ,

$$Jt = AF_1(h\nu)\left\{\int_{qV}^{\zeta p}\left[1 - \exp\frac{-2(\zeta p-E)}{\overline{E}_\perp}\right]dE - \int_{qV-h\nu}^{qV}\left[1 - \exp\frac{-2(\zeta p-E)}{E}\right]dE\right\}.$$

$$Jt = -AF_1\left\{h\nu - (\zeta p-qV) + \frac{\overline{E}_\perp}{2}\left[1 - 2\exp - \frac{2\zeta p-qV}{E}\right] + \frac{\overline{E}_\perp}{2}\exp\frac{-2(\zeta p-qV-h\nu)}{E}\right\}$$

since $h\nu > \zeta p \approx \overline{E}_\perp$; the last term may be neglected.

$$\therefore \quad Jt = -AF_1\{ h\nu - (\zeta p-qV) + \frac{\overline{E}_\perp}{2}[1 - 2\exp - \frac{2(\zeta p-qV)}{\overline{E}_\perp}] \} \qquad (31)$$

It can be easily seen that the first term is the current contribution from "excited holes", and is the dominant term at all bias, while the second term is from only those excited electrons that can find available states in the p-side. The last term depends strongly on applied bias voltage. At zero bias it is a positive term while at $qV = \zeta p$ it is a relatively larger negative term. The voltage dependence of the tunneling current for this particular case is shown in Figure 13.

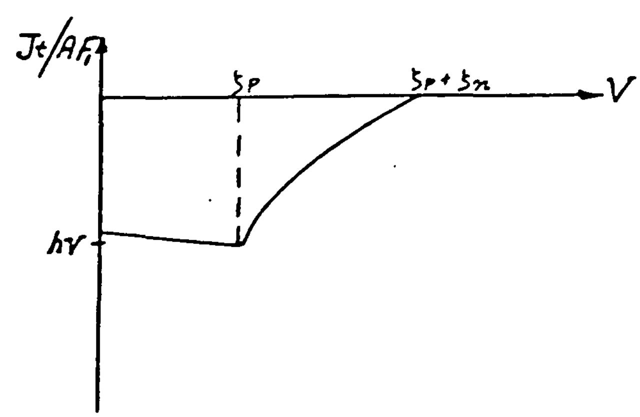

Figure 13 Case c : Current vs Voltage for $\zeta p < h\nu < \zeta n$.

III. 3.5 Magnitude of Excited Tunneling Current

To calculate an order of magnitude for the excited tunneling current, let us consider Case (c) where $\zeta_n > h\nu > \zeta_p \approx \overline{E}_\perp$. From equation (31), the maximum value of Jt is approximately

$$Jt\ max = -AF_1 h\nu \tag{32}$$

The D-C peak current is similarly evaluated at absolute zero temperature from equation (27) as:

$$J_{D-C} = A \int_0^{qV} \left[1 - \exp -2\left(\frac{\zeta p - E)}{\overline{E}_\perp} \right) \right] dE$$

$$J_{D-C} \approx A \left(\zeta p - \frac{\overline{E}_\perp}{2} \right) \quad \text{or}$$

if an order of magnitude is only wanted

$$J_{D-C} \approx A \zeta p \tag{33}$$

Thus the ratio of signal to D-C current is

$$Jt/J_{D-C} = F_1\, h\nu \,/\, \zeta p \tag{34}$$

From equation (15),

$$F_1 \simeq \frac{\Delta n}{N_D} \frac{\zeta_n}{h\nu}$$

Then
$$\frac{Jt}{J_{D-C}} \quad \frac{\Delta n}{N_D} \frac{\zeta n}{\zeta p}$$

where in general $\zeta n / \zeta p < 10$.

Therefore an order of magnitude for the currents ratio is given by

$$\frac{Jt}{J_{D-C}} \approx \frac{\Delta n}{N_D} \tag{35}$$

III. 3.5.1 Typical Parameters for a Germanium Tunnel Diode

The impurity doping densities are assumed to be

$$N_D = 2 \times 10^{19}/cm^3; \qquad N_A = 10^{19}/cm^3 .$$

Gap energy $E_G = 0.67$ ev.

Effective mass for an electron $m_e = .16\ m_o$

" " " a heavy hole $m_h = .40\ m_o$

" " " a light hole $m_\ell = .04\ m_o$

The tunneling effective mass is found to be the reciprocal sum of the electron and light hole effective masses [19]. Therefore the tunneling effective mass m* is given as,

$$\frac{1}{m^*} = \frac{1}{m_e} + \frac{1}{m_\ell} = \frac{1}{.032\ m_o} \qquad (36)$$

The fermi-level penetrations ζn and ζp are evaluated from the equation

$$\zeta n = \frac{h^2}{8m_e}\left(\frac{3}{\pi}\right)^{2/3} N_D^{2/3}$$

Substituting into the above equation appropriate values

$$\zeta n = .14 \text{ ev.}$$

Similarly

$$\zeta p = .04$$

By definition

$$\bar{E}_\perp = \frac{2\hbar e \mathcal{E}}{\pi m^* E_G^{1/2}} = .036 \text{ ev}$$

where $\mathcal{E}$, the electric field in the junction

$$= 4.6 \times 10^5 \text{ V/cm.}$$

In addition, the radiation from a CO_2 laser with photon energy $h\nu = 0.11$ ev. is absorbed in the degenerate germanium tunnel diode, the absorbtion coefficient $\alpha = 0.07 \mu m^{-1}$ as calculated in Appendix I. Also it is assumed that the power absorbed at the junction of the tunnel diode is 1 watt/mm^2. Then from equation (16), which gives Δn as,

$$\Delta n = \frac{\alpha I \tau}{h\nu}$$, and assuming a relaxation time of $\tau = 10^{-13}$sec, we get by substituting into equation (35)

that

$$Jt/J_{D-C} = 3.6 \times 10^{-8} .$$

If the D-C peak current is 20A, as in our diodes, the expected tunneling current due to the excitation of electrons by the laser is

$$It = 3.6 \times 10^{-8} \times 20 \approx 7 \times 10^{-7} \text{ A} .$$

This value of current is based on the assumption that the active cross-section areas of the two currents are equal and therefore the current responsivity $R_I = 7 \times 10^{-7}$ A/W. From the I-V characteristics, the diodes dynamic impedance is about $0.006\ \Omega$. Therefore an open circuit voltage equal to 4×10^{-9} volts and a corresponding voltage responsivity $R_v = 4 \times 10^{-9}$ V/W is expected as the signal generated due to excitation of electrons by laser radiation.

III. 3.5.2 Limiting factors in the Response Time

The basic parameters that would limit the speed of responseof the excitation signal are the energy relaxation time, the tunneling time, and the inherent RC time constant of the device.

The relaxation time as found in the literature [20] is of the order of 10^{-13} sec.

Franz [21] has on the other hand given an expression for the tunneling time through a rectangular barrier as:

$$\tau = \frac{h}{\sqrt{E_d}} \quad \frac{1}{2}\left(\frac{1}{\sqrt{E_1}} + \frac{1}{\sqrt{E_2}}\right) \qquad (37)$$

where E_1, E_2 are the kenetic energies of the particle before and after tunneling,

E_d = the barrier height wrt. the energy of the particle.

If the tunnel diode barrier is assumed to be rectangular for an order of magnitude calculation of the tunneling time, and

$$E_d = E_G = 0.7 \text{ ev}$$
$$E_1 = E_2 \approx E_F \simeq 0.1 \text{ ev} .$$

then, $\tau = 10^{-15}$ sec.

From the previous considerations, response times of 10^{-13} sec. can be expected. Thus the RC time constant will actually dictate the upper frequency limit of this device. Since tunnel diodes presently operate in the tens of gigacycle frequency region as oscillators and amplifiers [22], it is expected that the time response for the detection of modulated radiation will be in this range.

III. 3.6 Noise in Tunnel Diodes

III. 3.6.1 Introduction

Two significant scources of noise occur in tunnel diodes. First, the thermal or Johnson noise is associated with the spreading resistance R_s of the diode, and is taken into account by introducing an appropriate current or voltage generator ΔVt^2 at Rs in the tunnel diode's equivalent circuit, Figure 14. Secondly, shot noise will be produced by the bias current of the diode. As this current is determined by the diodes characteristics, the noise generator i_n^2 is introduced in parallel with gd the dynamic conductance of the device. In addition, there will be a noise generator i_L^2 associated with the equivalent load conductance g_L.

III. 3.6.2 Thermal or Johnson Noise

This type of noise originates from the random thermal motion of charged carriers in the conducting regions of the device. Its magnitude in terms of a mean square voltage is given as:

$$\Delta V_t^2 = 4 k_B TB/G_s \tag{38}$$

or in terms of current

$$\Delta i_t^2 = 4 k_B TG_s B \tag{39}$$

where G_s is the conductance of the material

T is the temperature

k_B is Boltzman's constant

B is the measuring instrument's bandwidth.

III. 3.6.3 Shot Noise in Tunnel Diodes

Shot noise is generated in the diode barrier as a result of two electronic currents flowing across the junction barrier in opposite directions. Electrons tunneling from the conduction band to the valence band give rise to a current which can be expressed as follows:

$$I_{c\rightarrow v} = A \int_{E_c}^{E_v} f_c(E)\, g_c(E)\, g_v(E)\, [1 - f(E)]\, T_{c\rightarrow v}\, dE \qquad (40a)$$

$$\equiv I_E \qquad ,$$

where f_i is the fermi function in band " i " ,

g_i is the density of states in band " i " ,

$T_{c\rightarrow v}$ is the transmission probability from conduction to valence band,

A is a proportionality constant.

Similarly the current from valence to conduction band is written as:

$$I_{v\rightarrow c} = A \int_{E_c}^{E_v} f_v(E)\, g_v(E)[1 - f_c(E)]g_c(E)\, T_{v\rightarrow c}\, dE \qquad (40b)$$

$$\equiv I_z \; .$$

The total external current is given by the algebraic sum of these currents as is shown in Figure 16.

However, since the individual shot noise currents are uncorrelated (to a first approx.) their noise contributions add on a power basis.

Let $Ieq = I_E + I_Z$ (41a)

but the measurable diode current $Id = I_E - I_Z$. (41b)

Assume that $T_{c \rightarrow v} = T_{v \rightarrow c}$.

By definition $f_c(E) = \dfrac{1}{1 + \exp(E - E_{F_n})/k_B T}$

and

$$f_v(E) = \frac{1}{1 + \exp\ (E - E_{F_p})/k_B T}$$

Also the external applied voltage given by $qV = E_{F_n} - E_{F_p}$

therefore $f_v(E) = \dfrac{1}{1 + \exp(E + qV - E_{F_n})/k_B T} = f_c(E + qV)$ (42)

Substituting expression (42) into equations (40), (41),

$$\begin{aligned} I_E &= A \int f_c(E)[1 - f_c(E + qV)\ ]\ \phi(E,V)\ dE \\ I_Z &= A \int f_c(E + qV)[1 - f_c(E)]\ \phi(E,V)\ dE \end{aligned} \qquad (43)$$

where $\phi(E,V) = g_c(E)\ g_v(E)$.

Now using the definition of $f_c(E)$ and some numerical manipulation

$$f_c(E + qV)\ [1 - f_c(E)] = f_c(E)[1 - f_c(E + qV)]e^{-qV/kT}$$

Substituting this expression into equation (43)

$$I_Z = I_E\ e^{-qV/kT}$$

Hence using equation (41b)

$$I_E = \frac{Id}{1 - e^{-qV/kT}} \quad ; \quad I_Z = \frac{Id}{e^{qV/kT} - 1} \qquad (44)$$

Thus $Ieq = I_E + I_Z = Id \coth qV/2kT$ (45)

From the above equation it is seen that if the applied voltage is greater than $\dfrac{kT}{q}$, $Ieq = Id$, the measurable bias current.

To find the shot noise current at zero bias, i.e. when $V \rightarrow 0$ and $Id \rightarrow 0$, equation (45) must be evaluated in the limit as $V \rightarrow 0$.

Then $\lim\limits_{V \to 0} \text{Ieq} = \lim\limits_{V \to 0} \left(\text{Id} \coth {}^{qV}/{}_{2k_BT} \right)$

$$= \lim_{V \to 0} \frac{\text{Id}}{\tanh qV/k_BT} .$$

By applying L'Hospital's Rule

$$\lim_{V \to 0} \text{Ieq} = \frac{2k_BT}{q} \left. \frac{d\text{Id}}{dV} \right/_{V = 0} \tag{46}$$

The noise current generator associated with shot noise has a mean square value

$$i_n^{\,2} = 2e \text{ Ieq } B \quad \text{when} \quad V \neq 0$$

and

$$\left. i_n^{\,2} = 4k_BTB\frac{d\text{Id}}{dV} \right|_{V=0} \quad \text{when} \quad V = 0 \tag{47}$$

Note that at zero bias the shot noise is equivalent to the thermal noise of a device with a dynamic conductance $\frac{d\text{Id}}{dV}$.

3.6.4 S/N Calculation for the Detector Circuit

Figure 15 shows a simplified form of Figure 14, where the spreading resistance Rs and the reactive components have been neglected. The signal generator $i_{A.C}$ has been inserted in parallel to the dynamic conductance gd of the tunnel diode, where $i_{A.C}$ is the excitation signal.

The shot noise power output of the diode detector is:

$$e^2d = \frac{id^2}{(gd + g_L)^2} = \frac{2q \text{ Ieq } B}{(gd + g_L)^2}$$

The noise power from the equivalent load conductance is:

$$e_L^{\,2} = \frac{4k_BT\ B}{(gd + g_L)} .$$

Thus the total noise power output is:

$$en^2 = ed^2 + e_L^{\,2} = \frac{2q \text{ Ieq } B}{(gd + g_L)^2} + \frac{4k_BT(gd + g_L)B}{(gd + g_L)^2}$$

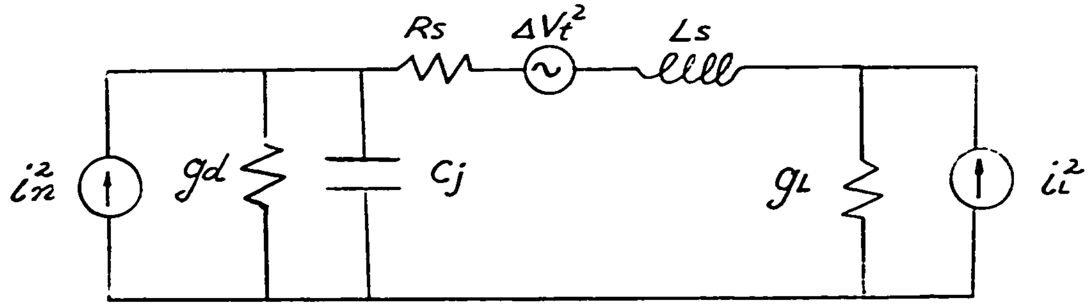

Figure 14 Tunnel Diode Equivalent Circuit

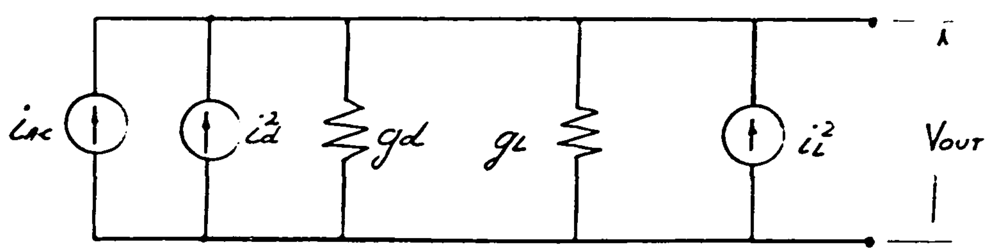

Figure 15 Detector Model

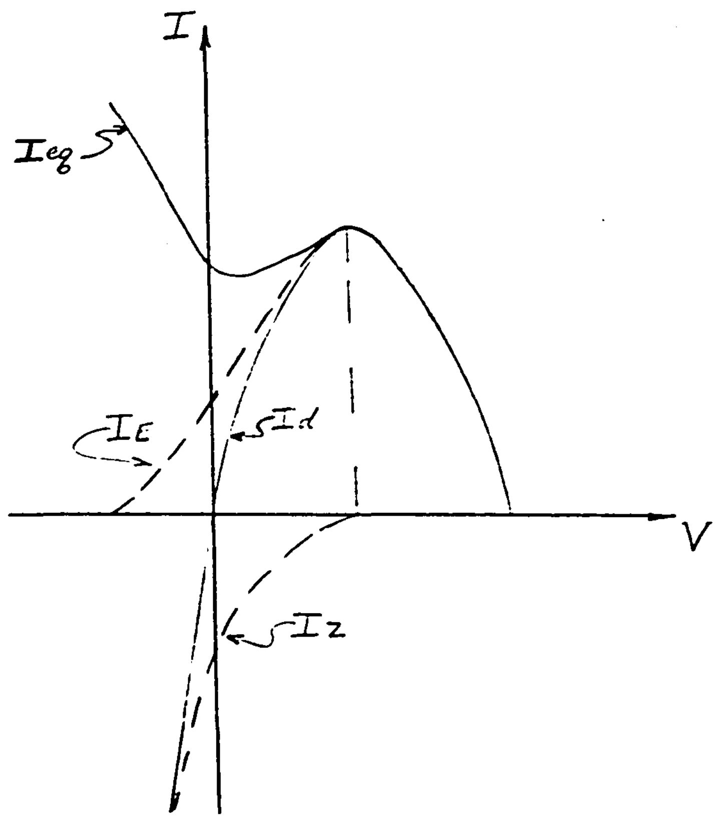

Figure 16 Shot Noise Current Components

The signal power output $e_{A.C}^2 = \dfrac{i_{A.C}^2}{(gd + g_L)^2}$

$$\therefore \quad S/N = \frac{e_{A.C}^2}{en^2} = \frac{i_{A.C}^2}{[\ 2q\ Ieq + 4k_B T(gd + g_L)\ ]\ B} \tag{48}$$

3.6.5 Numerical Value for S/N

Typical values for the parameters in equation (48) are:

$gd = 200\,\mho$, $\quad g_L = .001\,\mho$,

$k_B T = .04 \times 10^{-19}$ when $T = 300^o$ K

$I_{eq} = I_{D-C}$ when the applied voltage is greater than a few $k_B T$ as is shown in equation (45).

Thus $4k_B T(gd + g_L) = 3.2 \times 10^{-18}$

and $2q\ I_{eq} = 6.4 \times 10^{-18}$ when $I_{eq} = 20$ A .

Therefore it can bee seen that the two terms in the denominator are of the same order of magnitude. Thus equation (45) can be written in the form:

$$S/N = \frac{i_{A\ C}^2}{4q\ I_{eq}\ B} \ . \tag{49}$$

In section III, 3.5.1, it was shown that the excited tunneling current $i_{A\,C} \approx 7 \times 10^{-7}$ A . Therefore for unit bandwidth and an incident radiation level of 1 watt/mm^2, the

$$S/N = 4 \times 10^4 \ .$$

CHAPTER IV

Heating Effects

1.0 Introduction

In the previous analysis of the perturbation of the tunnel current produced by the excitation of electrons to a higher energy level due to the incident radiation, it has been implicitly assumed that the free carriers are loosely coupled to the lattice so that the energy they absorb does not raise the temperature of the sample. In otherwords, it was assumed that the radiation produced hot electrons whose effective temperature is above that of the lattice or the sample itself.

If the sample actually does undergo temperature change, two main thermal effects can produce additional electric signals. They are the thermoelectric or Seebeck effect which gives rise to a voltage ΔV if a temperature difference ΔT exists across the device according to the general relation $\Delta V = - \alpha \Delta T$ (50)

where α is the thermoelectric power, or Seebeck coefficient .

The second thermal effect is a bolometric action where essentially the resistance R of the device changes by ΔR with a change of ΔT in temperature , an incremental voltage thus appears across the sample

$$\Delta V = I \Delta R \tag{51}$$

where I is the current flowing in the device.

One important difference between the two effects is that the thermoelectric voltage is independent of bias, and exists even in the absence of the latter, whereas the bolometric effect depends entirely on the D-C operating point of the device.

IV. 2.0 The Thermoelectric Effect

The thermal behaviour of our tunnel diode device can be represented schematically as follows, and the physical structure of the diode is shown in Figure 19 .

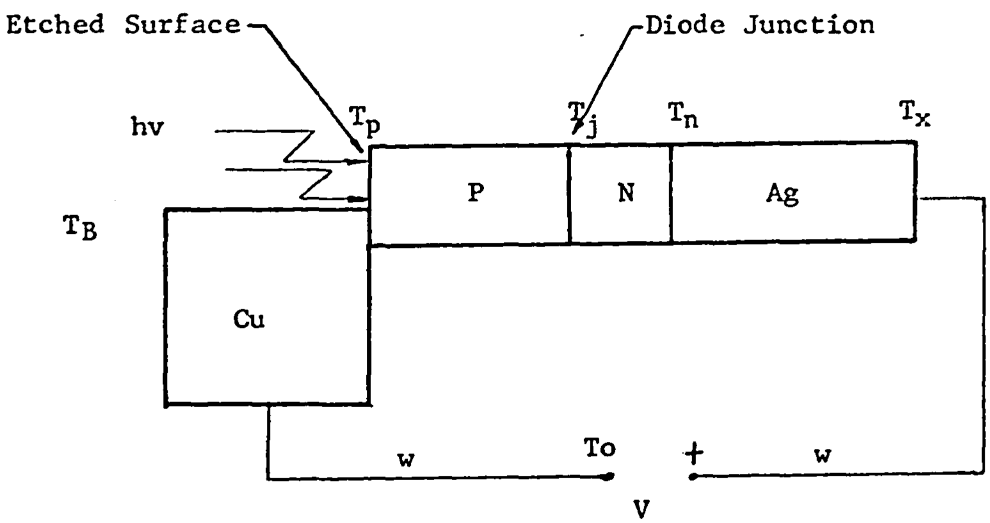

Figure 17.

Tunnel Diode Thermal Circuit

where PN is the diode itself, Cu is the copper casing of the diode and the connected heat sink; Ag is the silver lead attached to the alloyed N region; w represents the electric wires attached to a voltage measuring equipment. The various T's are the temperatures at their respective positions. Thus,

T_B is the temperature of the heat sink

T_p is the temperature of the exposed surface of the semiconductor,

T_j is the temperature at the junction of the diode,

T_n is the temperature at the junction of the n-type material and silver lead,

T_x is the temperature at the end of the silver lead,

T_o is the temperature of the measuring apparatus.

Now,

$$dV = - \alpha_i \, dT$$

where dV is the incremental voltage across a material of thermoelectric power α_i when an incremental temperature difference dT exists at its ends. Thus integrating around the circuit of Figure 17,

$$V = \alpha p \, (Tp-Tj) + \alpha n(Tj-Tn) - \alpha w(T_B-Tx) - \alpha cu(Tp-T_B) - \alpha Ag(Tx-Tn) \quad (52)$$

IV.2.1 Numerical Magnitude of the Thermoelectric Effect

For metals the values of α_i are [23]:

$$\alpha \text{ copper} = + 1.73 \ \mu V/K^o$$

$$\alpha \text{ silver} = + 1.35 \ \mu V/K^o$$

On the other hand a well known expression for extrinsic semiconductors is [23],

$$\alpha_s = \pm \frac{k_B}{q} \left[r_c + \frac{5}{2} + \ell n \frac{N_c}{N_t} \right] \quad (53)$$

where

r_c is in the order of unityand it depends on the phonon scattering mechanism,

N_c is the effective density of states in a band,

N_t is the impurity doping concentration.

The sign of αs is positive for p-type material and negative for n-type [23]. Since $N_c >> N_t$ for non-degenerate semiconductors their thermoelectric powers approach millivolts per degree.

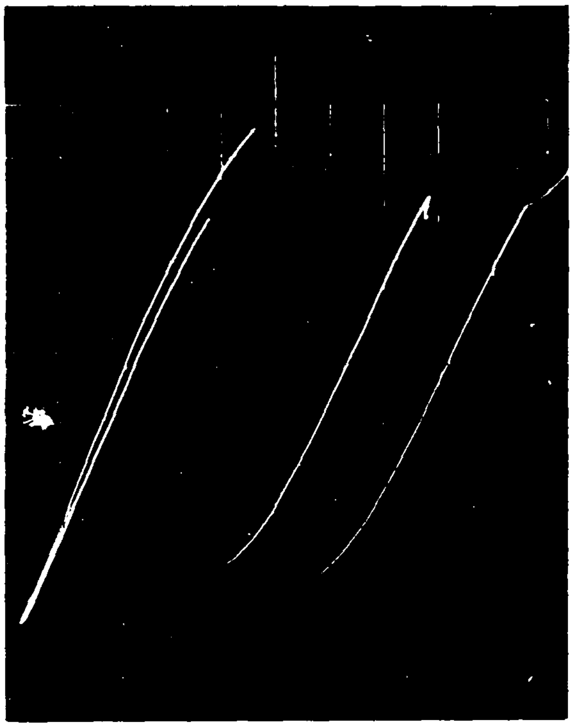

Vertical Scale: 2 Amp/Div

Horizontal Scale: 0.1 volt/Div

Figure 18 Temperature Dependence of I-V Characteristic

The trace with higher peak current and lower valley current corresponds to a temperature of $77^{o}K$. Other is at room temperature $\sim 300^{o}K$.

In our case the semiconductors are degenerate and their thermoelectric powers should be related to those of metals. As no definite values of the thermoelectric power for degenerate semiconductors could be found in the literature, approximate values are estimated as follows.

Theoretically [23] , the thermoelectric power of a metal is given as

$$\alpha m = \frac{-\pi^2 k_B}{2q} \frac{k_B T}{E_F} \tag{54}$$

This expression gives a value of $10\mu V/K^o$ at room temperature for a fermi level E_F of 1ev . Since the fermi-level penetration in tunnel diodes is typically 0.1 ev., the thermoelectric power is estimated to be $+100\mu V/K^o$ for α_p and $-100\mu V/K^o$ for α_n . This assumes that the degenerate semiconductors retain the same polarity sign for their α's as they possess in the extrinsic case.

Note that according to equation (54), these thermoelectric powers vary linearly with the ambient temperature.

IV. 3.0 Bolometric Effect

As was stated previously, this type of thermal effect is caused by a change in the resistance of a device or more rigourously a change in its I-V characteristic with temperature. The tunnel diode's I-V characteristic can be divided into three regions as is shown in Figure 4.

IV. 3.1 Region 1 - Current due to Band to Band Tunneling

The tunneling current in this region can be rewritten from equation (27) in the form

$$Jt = \text{const. } D \exp(-\alpha E_G) \tag{55}$$

where D and E_G are temperature dependent terms. The negative value of $\frac{\partial E_G}{\partial t}$ means the exponential term gives Jt a positive temperature coefficient. The quantity D is an overlap integral which determines the shape of the I-V characteristic in this region; it has the dimensions of voltage and depends on the depth of penetration of the fermi levels into the energy bands, ζn and ζp ; D will be essentially constant with respect to temperature as long as ζn and ζp are large compared to kT. For lightly doped diodes as in our case , the drop of D with increasing temperature reduces Jt since the fermi level penetrations decrease with increasing temperature, that is to say the semiconducting materials become less degenerate.

3.2 Region 2 - Excess Current

The excess current is mainly characterized by its exponential increase with voltage. It extends from the minimum current point of the I-V characteristic to the thermal current region. This corresponds to a voltage range equivalent to more than half of the band gap energy value.

The excess current density is expressed [24] as ;

$$J_{exc} = D'\exp\left[-\alpha'(E_G - eV + Q)\right] = D'\exp(-\alpha' V_j) \qquad (56)$$

The quantity Q is a function of the sum of the fermi level penetrations ($Q \approx .6(\zeta_n + \zeta_p)$, [24]). D' is a function of V and represents the variation of the density of impurity states with energy within the forbidden gap. The increase in valley excess current density is attributed to the variation of Vj in the exponential term which tends to increase the current with increasing temperature since both E_G and Q have negative temperature coefficients [IV, 3.1].

IV. 3.3 Region 3 - Thermal Current

At a large forward bias, the conductance is mainly determined by the thermal current, i.e. by the flow of carriers over the potential barrier due to the space charge region at the junction which is reduced when a forward voltage is applied; consequently, the diode current in this region should depend on voltage as exp(eV/akT), with $1 \leq a \leq 2$ in most common cases [25], [26]. For a conventional diode the current is expressed as:

$$J = Js \left[e^{qV/akT} - 1 \right] \tag{57}$$

where Js is called the saturation current density which has a very strong temperature dependence; it is defined as [27]:

$$Js = \text{const.}\ e^{\frac{-E_G}{kT}} \tag{58}$$

Since $E_G > V$, the saturation current term contributes mostly to the variation of the total current density with temperature. It is found that

$$\left.\frac{\partial V}{\partial T}\right|_{J,E_G} = -\frac{1}{T}\left(a\,\frac{E_G}{q} - V \right) \approx -\frac{1}{T}\,\frac{aE_G}{q} \tag{59}$$

In conclusion the I-V characteristic variation with temperature of a lightly doped degenerate diode can be summarized as shown in Figure 18, which shows an actual characteristic of a tunnel diode at room and liquid nitrogen temperatures. Notice that in the low voltage region the current variation with temperature is much less than in the excess and injection portion of the characteristic.

IV. 3.4. Numerical Magnitude of the Bolometric Effects

Our studies of the effect of temperature on the voltage characteristics show that the valley V_V and forward voltages V_F ,the latter being the voltage at which the excess-thermal currents equal the peak current, Figure 18, were reduced with increases in temperature at an average rate of approximately 0.8 to 1.1 mV/^{o}C respectively. These values compare to the voltage decrease with increasing temperature of conventional Si and Ge diodes, which occurs at a rate of approximately 2 mV/^{o}C [14] .

The smaller dV/dT coefficient of tunnel diodes than that of conventional diodes is attributed to the existance of appreciable excess current components at V_V and V_P ; the excess current being less temperature sensitive than the injection current component [14].

The peak voltage also decreases with increasing temperature but at the much slower rate of 0.1 mV/^{o}C. This temperature dependence of V_p is essentially due to the variation of the fermi-level penetration in the n- and p-regions with temperature.

In conclusion it can be generally said that the thermoelectric effect is expected to dominate in region 1 and is actually the only thermal effect at zero bias; on the other hand the bolometric effects are about an order of magnitude larger than the thermoelectric effect in regions 2 and 3.

IV. 4.0 Conclusions

Comparing the tunneling signal magnitude as estimated in III, 3.5.1 and the thermal effect magnitudes just determined, it appears that the latter are of larger magnitude ; but it is expected, however, that the thermal signals will have a relatively long response time, so that when the source beam is chopped at a relatively high rate, the thermal signals will be sufficiently attenuated to allow the observation of the previously described incremental changes in the tunneling current itself.

CHAPTER V

Experimental Results

V. 1.0 The Experimental Set-Up

V. 1.1 Introduction

The main components used in the experiment consisted of a CO_2 laser, a mechanical chopper, and a tunnel diode. The tunnel diode detector could be cooled to liquid nitrogen temperatures, being mounted on an insulated metalic box which acted as a dewar. This detector and dewar assembly was fastened onto a screw jack in order to be able to align with the laser beam. The set-up is shown in Figure 20.

V. 1.2 The Source of Radiation

A 10.6μm Holobeam series 20 CO_2 laser was used as a source of radiation for the experimental observations. Its power output was approximately 10 watts cw. Since the laser was being driven by an A-C power supply, the output power was in the form of a sixty-cycle full-wave rectified signal. The normal beam diameter of one centimeter could be focused, using a germanium lense of two inch focal length, to a diameter of about one millimeter.

V. 1.3 Modulation of the Laser Beam

The output beam of the laser could be modulated using a slotted rotating disc as a mechanical chopper. Actually the chopper consisted of two identical discs, mounted coaxially side-by-side, such that one of the discs could be rotated relative to the other in order to be able to vary the slot width and thus change the duty cycle anywhere from 1/2 to zero (see Figure 21). The maximum chopping obtained with the given disc motor assembly was one kilohertz.

V. 1.4 The Tunnel Diode Detector

1.4.1 The Diode Structure

The tunnel diodes used in the experiments were RCA type 40069. Their typical characteristics were I_p = 20A, V_p = .115 v, V_v = .340 v, I_v = 2.1A , and V_F =.525 v.

These high current diodes were used exclusively for their relatively large physical dimensions. The physical construction and dimensions of the diode package are given in Figure 19.

V. 1.4.2 Preparation

In order to be able to illuminate the surface of the semiconductor, a hole of diameter .025" was first drilled into the copper base reaching a depth just short of the p-type material. Then chemical etching was used to uncover the surface of the semiconductor and further etching of the semiconductor was possible when it was desired to get closer to the p-n junction.

V. 1.5 Etches

Basically, three different chemical etches were employed for various purposes. Nitric acid was used to etch the copper at the bottom of the drilled pilot hole. If at any time it was wanted to enlarge the exposed surface area of the p-semiconductor without removing any of it, acetic acid was utilized. It was found that this acid removed the copper slowly without affecting the semiconductor.

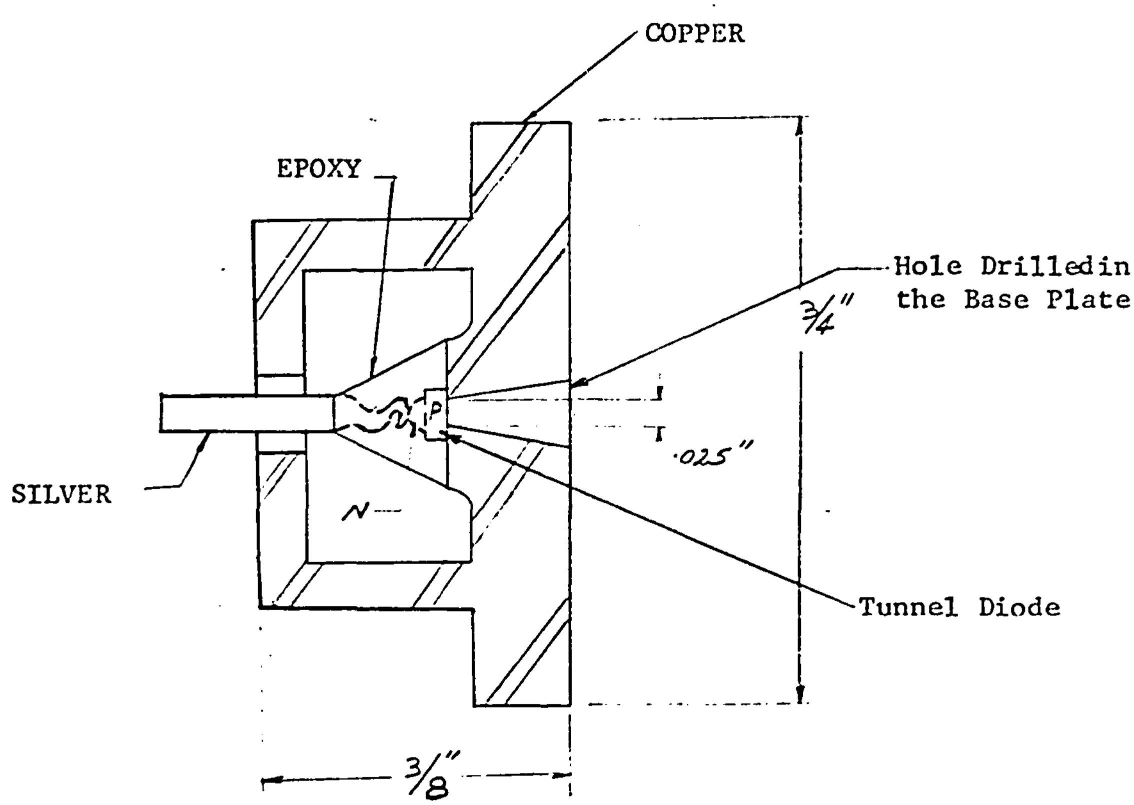

Figure 19   Diode Construction

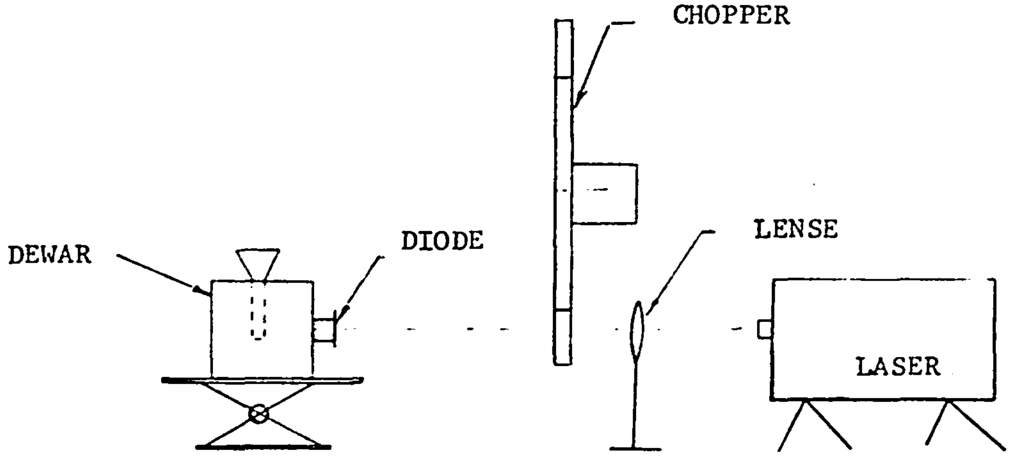

Figure 20 Experimental Set Up

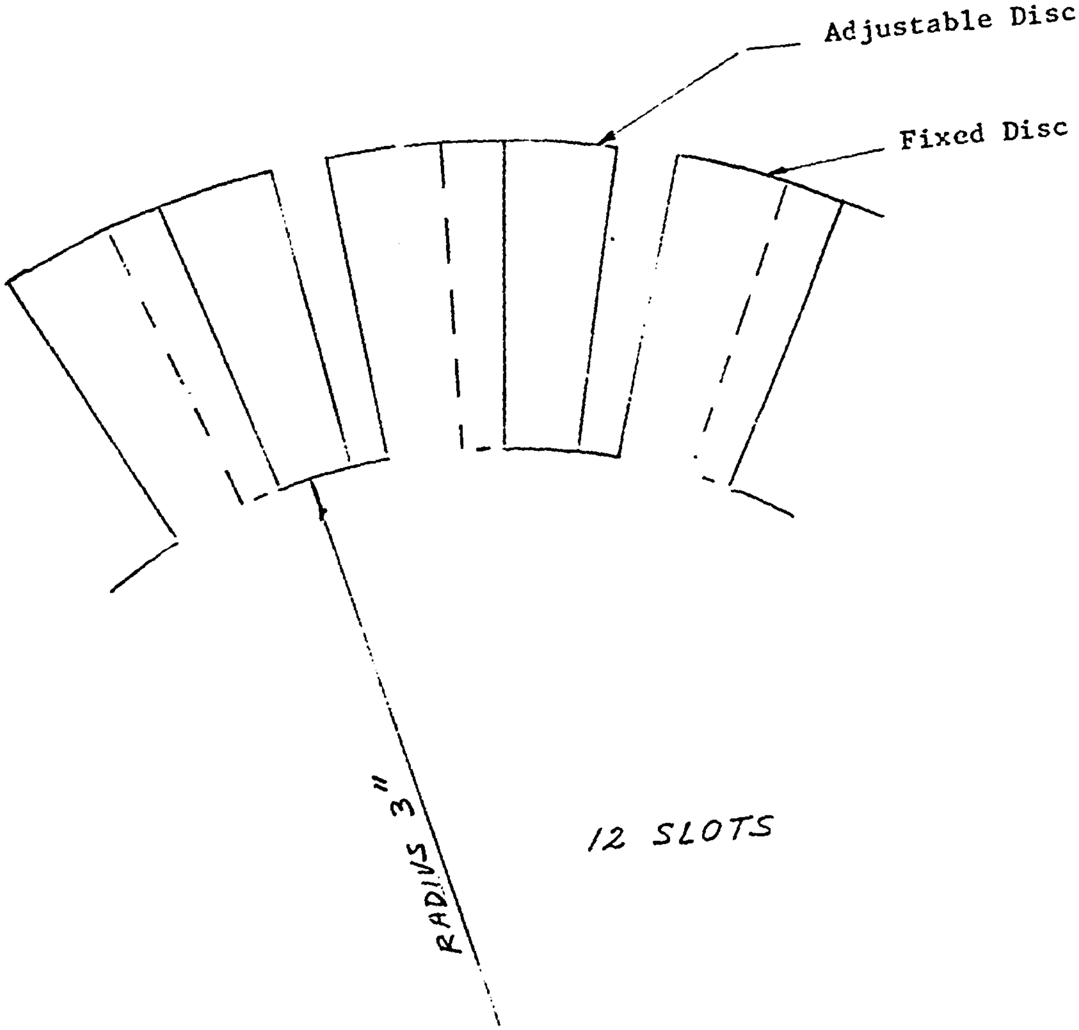

Figure 21 Chopper

In order to etch deeper into the semiconductor itself, the common CP-4 etch for germanium was used. It basically consists of 5 parts HNO_3, 3 parts HF, and 3 parts acetic acid. If a slower rate of etching was desired, the acetic acid content was increased.

The etching process had to be carefully monitored, since when the p-material was etched, the exposed surface area gradually enlarged to a point where there no longer was any contact left between the germanium and the copper base and thus the device became an open circuit.

V. 1.6 Effect of Etching on the Tunnel Diode Characteristics

It was found by Hall [28] and by this author that the etching of one side of the diode (in this case the p-side) caused only the peak current to diminish; since in our case the junction area remained constant, the decrease in peak current with etching is explained in terms of the band diagram of the tunnel diode as shown in Figure 22.

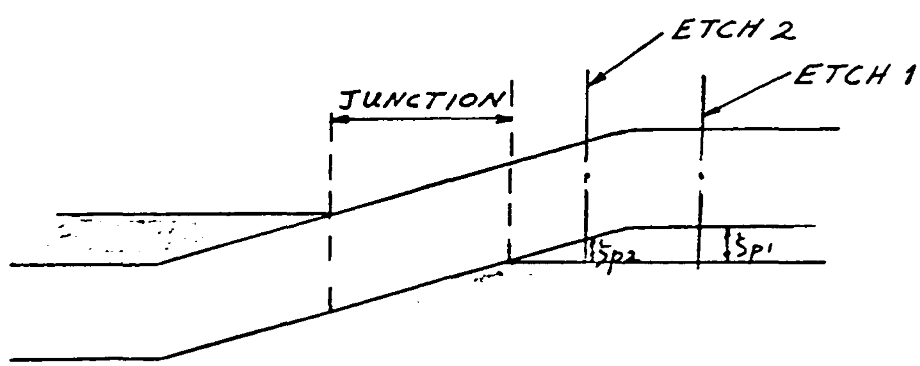

Figure 22 Junction Region of Tunnel Diode

An exploded view of the band diagram near the metallurgical junction is shown in the diagram. As can be seen, the closer one comes to the metallurgical junction, the less degenerate the germanium becomes as is indicated by the decrease of ζp which is the fermi-level penetration within the valence band. With the decrease of ζp, the number of available states, to which the n-side electrons can tunnel, also decreases, thus causing a decrease in the peak current. The valley and thermal currents are not affected as they do not depend on ζp to any great extent.

In general with the diodes used, the peak current could be reduced from 20 Amps. to 10 or 8 Amps. without losing electrical contact. Hall, in his paper, reports that with sufficient etching a conventional rectifying characteristics can eventually be achieved.

V. 1.7 Electric Circuitry

The circuitry used for the experiments is shown in Figure 23. At zero bias the circuit of Figure 23a was used; on the other hand, in order to bias the diode, the circuit of Figure 23b was employed. The change from one circuit to the other could be done with an appropriate switch.

In both circuits R_L has been conveniently chosen to be 1K. As far as the diode is concerned, the equivalent circuit of which is shown in Figure 14, R_L is actually an open circuit since both dynamic and static resistances are extremely small. Numerically the internal resistance of the diode, as deducted from its characteristics, is in the range of .005 to .015 Ω . Thus the diode acts as a low internal impedance scource; i.e. a voltage scource. Therefore practically for all R_L the measured voltage is the open circuit voltage of the tunnel diode.

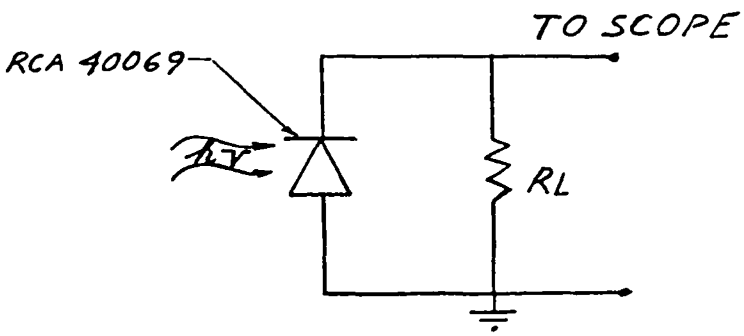

a) Zero Bias

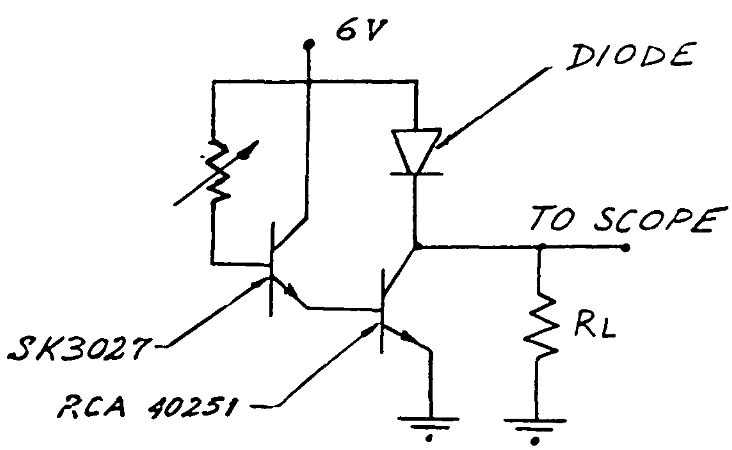

b) Bias Circuit

Figure 23 Electric Circuitry

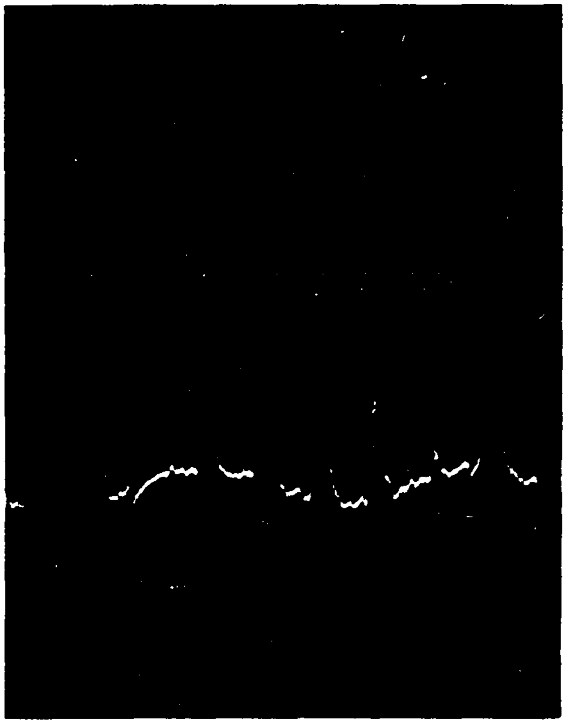

Vertical Scale: 20 μV/Div

Horizontal Scale: 2 msec./Div

Figure 24 Zero Bias Signal at 550 Hz

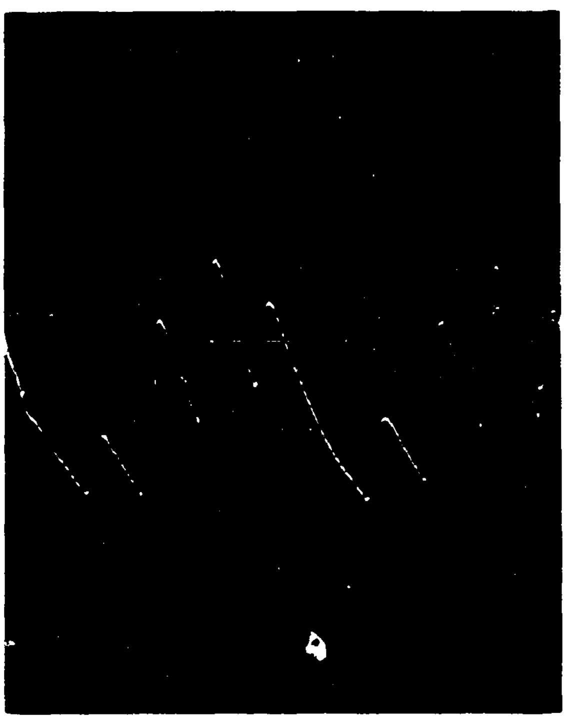

Vertical Scale: 200 μV/Div

Horizontal Scale: 2 msec./Div

Figure 25 Excess Current Signal at 550 Hz

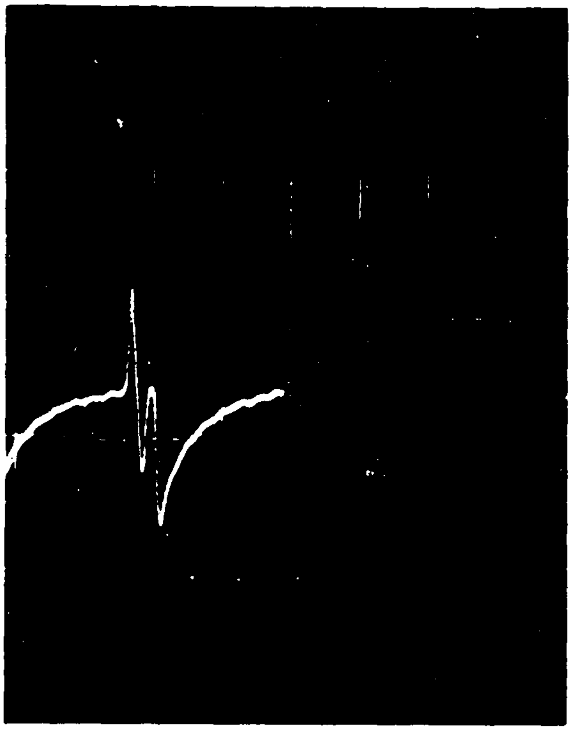

Vertical Scale: 50 μV/Div

Horizontal Scale: 20 msec/Div

Figure 26 Zero Bias Signal at 20 Hz

Vertical Scale: 20 μV/Div

Horizontal Scale: 2 msec/Div

Figure 27 Zero Bias Signal - Diode Etched

Vertical Scale: 20 μV/Div

Horizontal Scale: 2 msec/Div

Figure 28 Zero Bias Signal near Peak Current

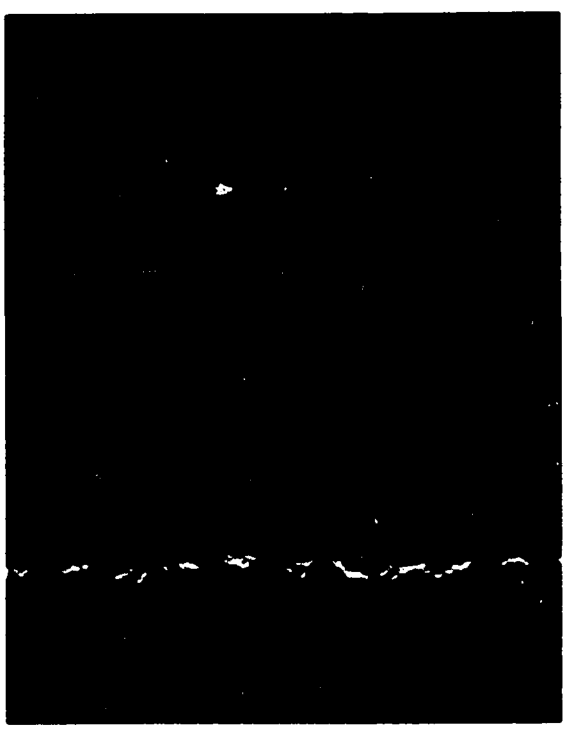

Vertical Scale: 10 μV/Div

Horizontal Scale: 2 msec/Div

Figure 29 Zero Bias Signal 550 Hz - N_2

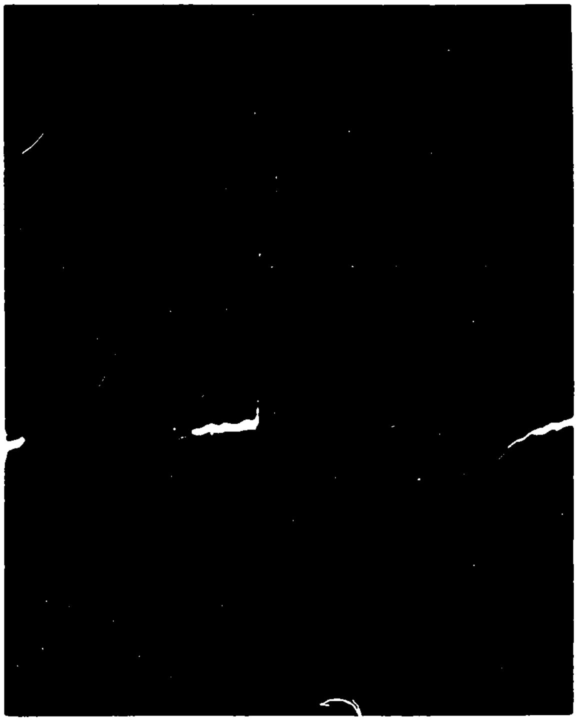

Vertical Scale: 25 μV/Div

Horizontal Scale: 20 msec/Div

Figure 30 Zero Bias Signal
20 Hz - N_2

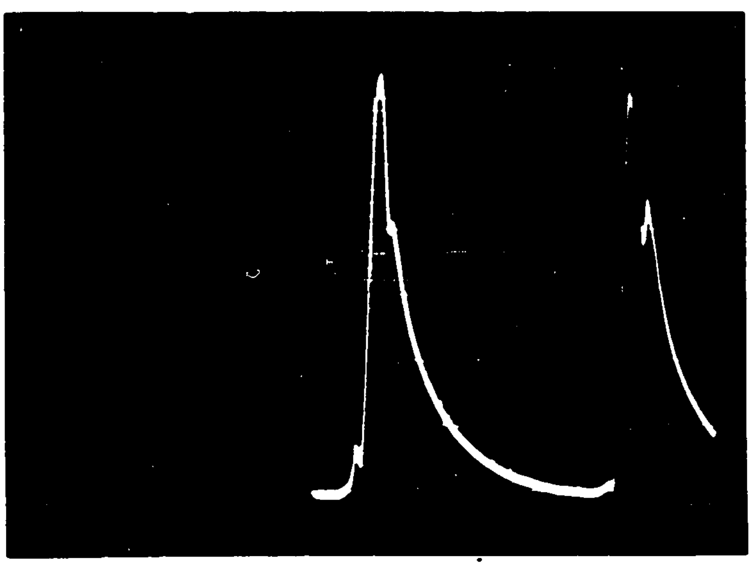

Vertical Scale: 1 mV/Div

Horizontal Scale: 20 msec/Div

Figure 31 Valley Signal at 20 Hz

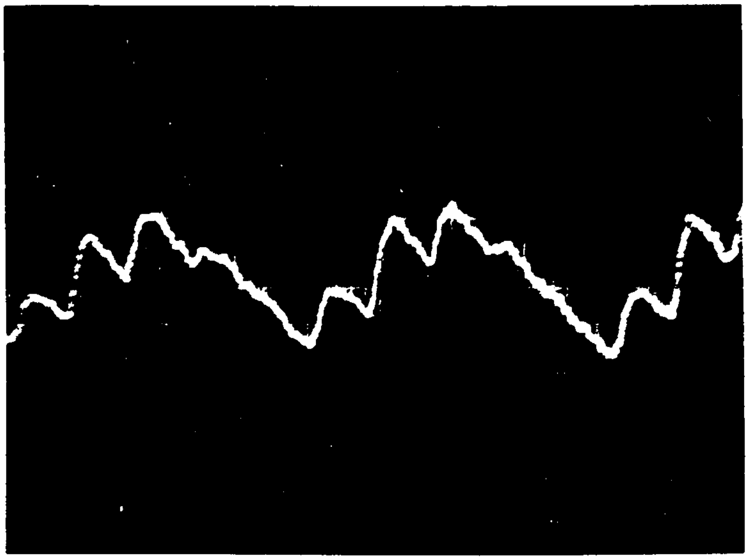

Vertical Scale: 200 μV/Div

Horizontal Scale: 2 msec/Div

Figure 32 High Etching - High Current Signal

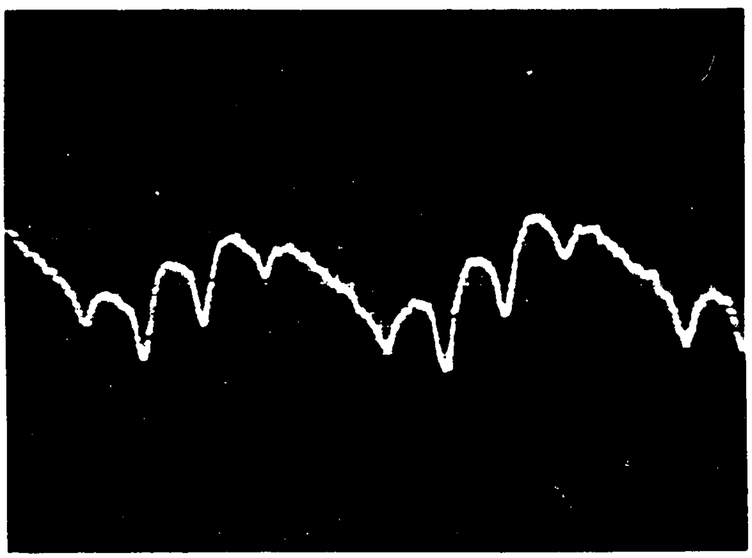

Vertical Scale: 200 μV/Div

Horizontal Scale: 2 msec/Div

Figure 33 High Etching - Medium Current Signal

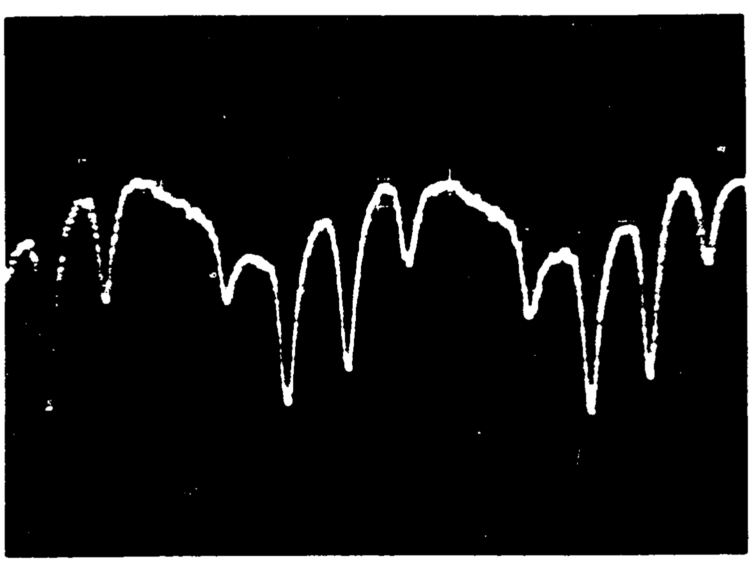

Vertical Scale: 200 μV/Div

Horizontal Scale: 2 msec/Div

Figure 34 High Etching - Valley Current Signal

The transistor circuit of Figure 23b serves as an adjustable constant current scource. Also the second transistor (type 40251) is used in order to dissipate the high power which is developed when the six volt car battery delivers up to 20A currents through the diode.

V. 1.8 General Experimental Procedure

The exposed surface of the p-type semiconductor is illuminated with the radiation from the CO_2 laser. The resulting electric signals were monitored on an oscilloscope, (Tektronix Type 532 with plug-in unit 1A7A). This plug-in unit has a sensitivity of up to 10μV/div., and variable upper and lower frequency cut-off points.

Measurements were done both at room and liquid nitrogen temperatures These measurements were repeated at gradually increasing levels of etching of the semiconductor device which brought the tunneling junction closer and closer to the exposed surface of the device. Changes in magnitude and response time of the signal at the diode terminals were observed at these different etching levels.

V. 2.0 Observed Results

V. 2.1 Introduction

Two basic types of signals were observed when the tunnel diode was illuminated with a chopped laser radiation. These signals are shown in the oscillograms of Figures 24 and 25. It must be pointed out that the envelope of the peak magnitudes of the signal originates from the inherent 60 cycle full wave rectified waveform modulation of the laser power as stated in section V, 1.2. Figure 24 shows the zero bias signal, while Figure 25, the signal when the diode is biased in the excess current region.

All polarities of signals mentioned in the text to follow are with respect to the p-side of the diode. In other words, "a positive signal" implies that the n-side of the diode is at a higher potential than the p-side.

V. 2.2. Zero Bias Signal

It is found that the decay time constant of the positive signal is about 300-500μsec. This positive zero bias signal, at a chopping frequency of 550 Hz is superimposed on a negative D-C value of approximately 10μV, which increases to about 80μV with the etching of the semiconductor. In addition, as seen in Figure 24, the base line is modulated by a slower negative signal which is found to increase with etching (Figure 27). This ripple on the base line tends also to increase if the bias current approaches the peak current (Figure 28) especially after considerable etching of the semiconductor.

When a chopping frequency of 20 Hz is used, a signal such as in Figure 26 is obtained. The negative A-C signal has a decay time constant of about 15msec. and its magnitude is nearly equal to the superimposed positive signal. In this case essentially no D-C signal components is observed anymore.

V. 2.2.1 Effect of Ambient Temperature

In general it was noted that the magnitudes of all the signals decreased when the diode detector was cooled to near liquid nitrogen temperature, although in some diode samples, the amplitudes of the positive signals remained constant if large radiation power densities were used. At all power levels, it was also observed that the ratio of positive to negative A-C signals increased at all chopping frequencies at liquid nitrogen temperature as shown in Figures 29 and 30; notice the small ripple on the base line of the positive signal at 550 Hz in Figure 29, and the relatively smaller negative A-C signal in Figure 30 compared to Figure 26. In addition a large negative D-C component appeared at liquid nitrogen temperatues which was independent of the chopping frequency.

V. 2.3 Signal in the Excess Current Region

V. 2.3.1 Signal at Small to Moderate Etching

The oscillograms of Figures 25 and 31 illustrate the signal generally obtained at both 550 Hz and 20 Hz when the diode is biased in the excess injection current region of the I-V characteristic. The magnitudes of these signals are always approximately ten times larger than the zero biased signal, and their time constant is about 15msec. These signals appeared to be independent of etching and were found to increase significantly only as the biasing approached the valley region. When the etching depth became very large, however, the response of the tunnel diode in the valley region has often changed drastically as next described.

V. 2.3.2 Signals at Higher Etching Levels

When the diodes in question had been etched deep enough such that their peak currents were at or below 10 A, signals such as shown in Figures 32, 33, and 34 were obtained. These photographs show that as the bias is decreased from high current to the valley region, the signal gradually changes from its previous form to a relatively fast (time constant =400 μs) and most importantly, an opposite polarity signal.

V. 3.0 Analysis of Results

V. 3.1 Introduction

The response of the tunnel diode due to the perturbation of the tunneling current by the incident radiation as was analysed in Chapter III was found to be overwhelmed by signals, as presented in section IV, 2.0, of larger magnitudes and longer time constants. The signal appearing in the excess current region could easily be attributed to a bolometric effect due to its relatively long time constant and correct polarity. It was, however, difficult to relate the zero bias signal to a thermal effect because of its vastly shorter time constant relative to the signal obtained in the excess current region, and its opposite polarity to the superimposed D-C signal (Section IV, 2.2) which itself was naturally attributed to a thermoelectric effect. If the signals, in the two regions of the I-V characteristics, arose from a thermal effect, they would be expected to have similar response times as both should result from the heating and cooling of the same diode structure. In other words, the device as a whole should have a certain thermal time constant which would be common to all thermal signals. Thus, in order to explain the mechanism for the relatively fast and large magnitude zero bias signal, a modified theory of tunneling with the possibility of intervention of slow gap states was first investigated.

V. 3.2 Discussion of the Zero Bias Signal

V. 3.2.1 Modified Tunneling Theory

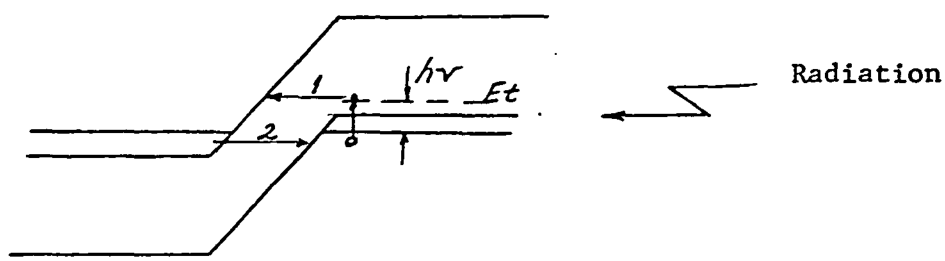

Figure 35 Modified Tunneling Theory

It was proposed that the electrons excited by the radiation incident on the p half of the tunnel diode (Figure 35) were first excited to allowed trap energy states Et within the forbidden energy gap region situated at an energy level $h\nu = 0.1$ ev. above the local fermi-level. This trap level Et could be due to either impurity, dislocation or any lattice defects which are always present in the crystal near the junction. Once the electron has been excited to this level, two types of tunneling currents can be considered (see Figure 35).

V. 3.2.1a Component One:

This component can arise when the electrons tunnel from the trap level into the conduction band of the n-type material. This mechanism is very improbable since electrons in discrete energy levels have almost no kinetic energy which is essential for tunneling to take place. There exists the slight possibility that these energy levels are of sufficient concentration to form a band that is separated from the valence band itself and thereby the electrons are allowed to have sufficient kinetic energy to tunnel. This type of current, however, gives a signal polarity opposite to that observed under zero bias conditions.

V. 3.2.1b Component Two:

The second possible process eliminates all the previous objections. In this case, once an electron has been excited to the trap level, it leaves also an additional available state behind in the valence band, to which now an electron from the conduction band on the n-side of the junction can tunnel. Although this type of tunneling current satisfies the observed polarity condition, the lifetimes or recombination times between the trap level and valence band must be examined since this time governs the speed of response.

The possible types of gap states that normally arise, are neutral donors and acceptors, positively charged donors or negatively charged acceptors [29] . From theoretical calculations (see Appendix II), it is found that a capture cross-section of approximately $10^{-22}cm^2$ is needed to obtain the observable lifetime of 300μsec. The only type of impurity that could have such a capture cross-section for the recombination process involved, is a positively charged or even doubly positively charged donor type impurity [29]. It also must exist close to the valence band since the excitation energy of the radiation is 0.12 ev.

That this type of level exists is very improbable from known data on germanium semiconductors. Even if such states did occur, they would be present in minute concentrations and thus signal saturation effects should be observable; this is not the case experimentally, and therefore impurity assisted tunneling currents had to be ruled out as the cause of the observed signal. The only alternative left to explain the zero bias signal is a special case of the thermoelectric effect since this is the only other effect that can exist at the zero bias condition.

V. 3.2.2 The Zero Bias Signal - Thermal Effects

The thermal equivalent circuit for the tunnel diode package is shown in Figure 17.

From section 2.0 in the previous chapter the thermoelectric voltage is given in equation (52) as:

$$V = \alpha_p (T_p - T_j) + \alpha_n (T_j - T_n) - \alpha_{cu}(T_p - T_B) - \alpha_{A_G}(T_x - T_n) - \alpha_w(T_B - T_x)$$

Radiation is absorbed in the region near the copper-germanium interface. It is believed that the relatively fast positive response signal at zero bias is due to the thermoelectric effect resulting from the change in the temperature of only the surface of the p-material. In other words, the surface temperature T_p can change at a faster rate than a bulk temperature such as T_j.

The thermoelectric voltage equation for A-C signals can be acquired by rewriting the previous equation in the following form when relative time constants are included.

$$\Delta V(\omega) = \frac{\alpha p \Delta Tp}{1+(\omega\tau_1)^2} + \frac{(\alpha n - \alpha p)\Delta Tj}{1+(\omega\tau_2)^2} - \frac{\alpha n \Delta Tn}{1+(\omega\tau_3)^2} \qquad (60)$$

where τ_1 is the thermal time constant associated with the surface of the p-material

τ_2 is the thermal time constant associated with the junction area of the n and p materials,

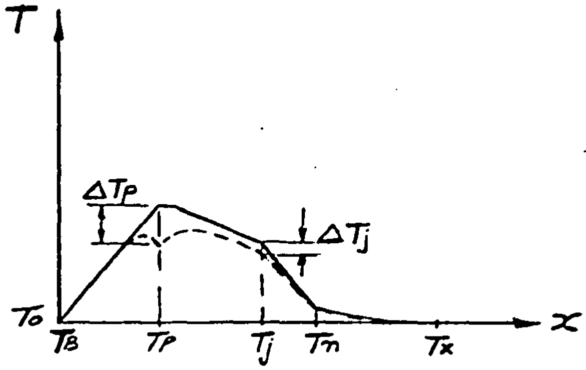

Figure 36 Temperature Distribution

—— Equilibrium temperature distribution

- - - A-C change wrt to equilibrium distribution when radiation is chopped

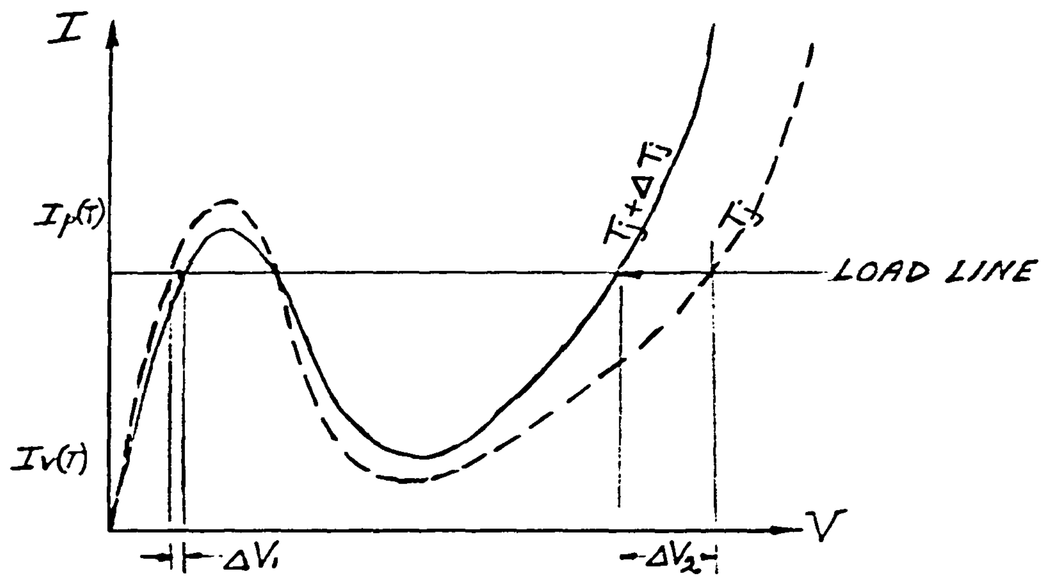

Figure 37 Temperature Variation of I-V Characteristic

τ_3 is the thermal time constant associated with the junction area of the n-material and silver lead

and $\tau_1 < \tau_2 < \tau_3$.

The remaining terms have been neglected since the corresponding α's are two orders of magnitude smaller. In fact, ΔT_n can also be assumed to be zero since the silver lead acts as an adequate constant temperature bath; thus, only the first two terms are significant in equation 60.

Since the first two terms in equation (60) are of opposite sign ($\alpha_p = -\alpha_n$), and with different time constants, the net output voltage is a superposition of the two signals. The first term (positive polarity) dominates at chopping frequencies above τ_2^{-1} while at frequencies below τ_2^{-1} the signal tends to become more negative as $\alpha_p - \alpha_n \simeq 2\alpha_p$.

Figure 24 shows the output signal being chopped at a frequency of 550 Hz at zero bias. The positive peaks are the signals arising from temperature change on the surface of the p-type germanium, i.e. the term $\alpha_p \Delta T_p$. The time constant associated with this positive signal is found to be 300-500μsec. The modulation of the base line is attributed to the slower signal caused by the junction temperature T_j changing, i.e. the second term in equation (60).

Figure 26 shows the signal detected when the laser output is chopped at a frequency of 20 Hz . Here the contribution from the two different signals is more distinct. The negative portion arises from the second term in the equation, while the laser's modulated power appears as the positive spikes. The decay time constant of the negative signal is 10-

15msec and is attributed to the time necessary for the junction and bulk temperature T_j to change.

Since the variation of the junction temperature Tj determines the temperature of the tunnel diode's I-V characteristic, any A-C signal that is attributed to the bolometric effect, caused by the diode being heated by radiation, must have the thermal time constant associated with the junction temperature.

Figure 28 shows the detector's signal when biased in the direct tunneling region. The negative component of the signal is the result of the addition of that thermoelectric voltage which depends on ΔTj and the bolometric effect which also depends on the same temperature change. The two effects are of the same polarity, time constant and order of magnitude. As can be deducted from the I-V characteristic diagram, the bolometric portion of the signal should increase as the peak current is approached. This factwas substantiated experimentally.

V. 3.3. Effect of Etching on the Zero Bias Signal

The thickness of the p side of the tunnel diode is approximately 400 μm. Most of the power is absorbed in a tenth of this distance as the calculated absorbtion constant is $0.07 \mu m^{-1}$,(see Appendix I). Thus, in general, $\Delta Tp > \Delta Tj$. As the thickness of the p-side is reduced by chemical etching, ΔTj approaches ΔTp and thereby the negative portion of the signal increases. This trend is illustrated in Figure 27 which shows the output signal after some etching. Note the increase in thenegative signal as depicted by the larger modulation of the positive signal base line.

V. 3.4 Detector Output with Bias Current

V. 3.4.1 Introduction

Bias dependence of the detector's signal is divided into two regions. The tunneling part of the characteristic, (from zero bias to peak current) constitutes the first region, while the second includes bias currents from the valley to higher currents in the injection part of the characteristic.

As a bias is applied, bolometric effects are observed in the detected signal. Recall that the bolometric effect can be depicted as the temperature dependence of the I-V characteristic.

V. 3.4.2 Tunneling Region

As was explained in section IV, 3.1, the peak current in lightly degenerate tunnel diodes, decreases with an increase in temperature.

When radiation heats the diode and changes its temperature, the change in the tunneling current due to its temperature dependence, is observed as a voltage ΔV when the diode is biased at a constant current as is shown in Figure 37. Due to the nature of the electric circuitry (Figure 23), ΔV appears as a negative voltage on an oscilloscope. This voltage is naturally superimposed on the signals generated by the previously discussed thermoelectric effect which is independent of biasing.

V. 3.4.3 Detected Signal in the Excess Current Region

As stated in the theory in section 3.4 of the previous chapter, bolometric effects were expected to dominate in the excess and injection current portion of the tunnel diode's characteristic. The I-V characteristic is shown in Figure 37 at two different temperatures.

When the diode is biased such that the current remains constant, i.e. the load line is horizontal, any change in the I-V characteristic due to the temperature inerease caused by the heating effects due to the absorbed laser radiation, results in the appearance of a voltage change. Notice that the voltage change generated in the tunneling region ΔV_1, is of opposite polarity to the corresponding voltage ΔV_2 in the excess current region.

The comparison of the magnitudes of the signal in Figure 25 to the magnitude of the negative portion of the signal in Figure 28, confirms the theoretical prediction in section IV, 3.4, that the bolometric effect in the excess current region is one order of magnitude larger than the bolometric effect in the tunneling part of the I-V characteristic. From Figure 31, the decay time constant for this bolometric effect is found to be 10-15msec, which is equal to the decay time constant of both the bolometric signal in the tunneling region of the diode's characteristic and the negative part of the thermoelectric signal at zero bias, Figure 26. This fact is consistant with the theory presented in Chapter IV that all three of these signals are attributed to changes in the junction temperature T_j.

V. 3.5 Ambient Temperature Dependence of Detected Signals

In general, the detected signals decreased with a decrease in ambient temperature. The time constants within the limit of experimental accuracy remained unchanged.

The decrease of the thermoelectric portion of the signal is attributed to the temperature dependence of the thermoelectric power coefficients for degenerate semiconductors α_n and α_p as was shown in equation (54).

In the region where the characteristic is the summation of both excess and thermal injection currents, as the temperature is decreased, the excess current which is less temperature sensitive than the injection current, becomes more and more dominant. Therefore a smaller signal will be generated when the diode is heated by laser radiation at lower ambient temperatures.

Also at liquid nitrogen temperatures, T_B is much lower than the other. temperatures defined in equation (52), since it corresponds to the temperature of the heat sink which is in direct contact with the liquid nitrogen while the other temperatures are higher due to the fact that their corresponding positions are influenced by the ambient room temperature. Thus the large negative D-C voltage (refer to section V, 2.2.1), which was found to be independent of chopping frequency, is attributed to the term- α_{cu} $(Tp - T_B)$ in equation (52) as $T_p > T_B$. This signal, for practical purposes, is frequency independent due to the large thermal time constant associated with the heat sink.

V. 4.0 Valley Signal Polarity Reversal at High Etching Levels

Figures 32, 33, and 34 show as described in section V, 2.3.2, the output signal obtained from some of the diodes which have been considerably etched when the bias is changed from a high value to the valley point.

It has been observed that when such signals are present, the valley currents of the diodes are increased above their normal value. The valley currents, as stated in section IV, 3.2, are strongly influenced by the presence of energy gap states; it is expected that as the diodes are etched, the surface of the semiconductor naturally approaches the junction area, and any surface states that are present due to surface defects or contamination, will provide available tunneling states in the forbidden gap region which results in the increase of the excess current, see Figure 38a.

When the surface of the diode is illuminated with the laser radiation, (Figure 38b), the number of empty gap states, to which normally electrons would have been able to tunnel, is decreased due to either thermal or direct excitation of electrons to these levels, thus reducing the excess current.

The reduction of the excess current in the presence of surface states and with the radiation on, would clearly result in a negative voltage with respect to our electric circuitry. It is expected that the degree of occupation of the gap states lying within 0.1 ev. of the valence band, in the case of direct excitation, or within a few kT of the Fermi-level,in the case of thermal excitation, would in particular be affected by the radiation. In addition, as stated in section IV, 1.6, the Fermi-level approaches the valence band near the junction region, and therefore it can be safely assumed that at high etching levels, the Fermi-level practically coincides with the edge of the valence band. Thus, it is expected that the signals due to the perturbation of the occupation of surface states, should increase as the bias approaches the valley region of the diodes I-V characteristic.

Experimentally it has been observed that the excess current of a diode is increased with the intentional introduction of surface states by the application of non-distilled water or by the mechanical damage of the exposed surface [37] of a diode. When this increase of the valley current occurs, only then will the diode exhibit the signal polarity reversal in the valley region as shown in Figure 34; also, notice that the increase in the negative signal as the valley is approached is in accordance with the statements presented in the previous paragraph.

Following the removal of the introduced surface states by slight etching the valley current decreased to its original value, and the negative signal no longer appeared. This cycle could be reproduced at will.

Since the time constant of the excitation signal ($\approx$ 400μsec) is similar in value to that of the positive signal obtained at zero bias, it is concluded that the change in the density of available gap states is a surface effect caused by the population of the surface state levels by the thermal excitation of electrons, rather than by direct excitation. Indeed the perturbation of surface states by direct excitation of electrons to these levels, necessitates capture cross-section of the same order of magnitude as estimated in the modified theory of tunneling, section V, 3.2.1.

V. 5.0 Conclusions

It has been found that the observed signals were the combined result of several thermal effects. At zero bias, it is considered that the signals are thermoelectric in nature, with the relatively fast positive signal which has a response time in the order of 400μsec, due to the fast thermal response time of the surface layers of the exposed diode structure.

Under biased conditions, bolometric signals are also measured in the two portions of the diode's I-V characteristics, with the signals in the excess current region being one order of magnitude larger than those in the tunneling part. These signals exhibit decay time constants of 10-15msec. and are attributed to the temperature variation of the junction area of the diode.

At high etching levels, and with the presence of surface states, a signal with a reversal in polarity and with a relatively short time constant of 400μsec is obtained in the excess current region. This behaviour is explained as radiation induced thermal modulation of the tunneling current at the junction into surface states.

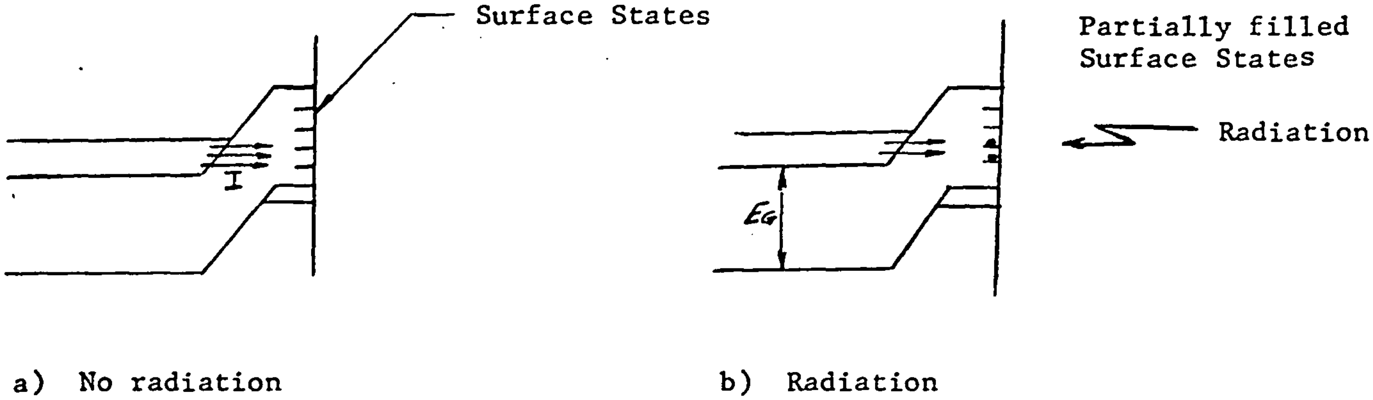

Figure 38 Surface States

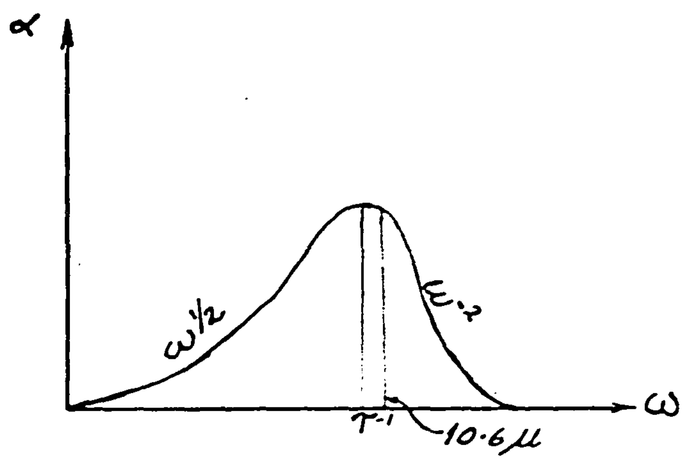

Figure 39 Absorbtion Coefficient vs Radiation Frequency

CHAPTER IV

Conclusion

This thesis constitutes a theoretical and experimental study of the response of a germanium tunnel diode to incident sub-energy gap radiation. The perturbation of the tunneling current by the incident radiation has been evaluated in detail expecting eventually to use this effect as a means of detecting submillimeter radiation at room temperature and with a high frequency response. A signal to noise ratio of 4×10^4 per unit bandwidth is expected for an incident power of 1 watt per mm^2.

It has been experimentally found, however, that this effect at modulation frequencies up to a few kilohertz, is buried in signals originating from thermal effects.

The observed thermally generated signals have been classified as a surface thermoelectric effect with a relatively high frequency response of few kilohertz, bolometric effects having about two orders of magnitude slower response times, and thermally perturbed tunneling currents due to surface states, having a few kilohertz frequency response.

It is thus concluded that the perturbation of tunneling currents in normal tunnel diodes is expected to be a convenient means of detecting submillimeter radiation only if high power, short duration (less than 1 μsec) laser pulses are used. Much better results however are expected from tunneling MOS structures because of the better control in the site of the absorbed radiation and the much higher internal impedance [10] of this device which results in larger signal voltages compared to the signals obtained from the very low impedance tunnel diodes.

APPENDIX I

Free Carrier Absorption

As is well known, the absorption of a photon by an electron in a perfect crystal is a forbidden process. The electron can gain a large amount of energy but very little momentum from the photon. In order for absorption to occur, then, the electron must gain momentum from some lattice imperfection namely through phonon scattering. Several authors [17], [30], [31] have treated this problem theoretically using quantum mechanics and attempting with limited success, to fit their theories to the experimental data of workers as Fan, Spitzer, and Collins [32]. The classical approach to this absorption problem developed by Drude [33], in general is adequate and will be used to calculate the absorption constant of free carriers in this work.

According to Drude, the free carrier absorption can be calculated from the following equations:

$$n^2 - k^2 = n_c{}^2 - \frac{Ne^2}{m^* \epsilon_o} \frac{1}{\omega^2 + g^2} \tag{61}$$

$$2nk\omega = g \frac{Ne^2}{m^* \epsilon_o} \frac{1}{\omega^2 + g^2} \tag{62}$$

where

n - real part of the refractive index

k - the imaginary part of the refractive index

n_c - constant refractive index in the non-despersive region $n_c^2 = \epsilon = 16$ for Ge.

N - number of free carriers

ω - radian frequency of incident radiation

m^* - is the effective mass of the free carrier

ϵ_o - is the permittivity of free space

μ - is the mobility of the particle

g - is the reciprocal of the relaxation time

Sample Calculations for α

1) For radiation 10.6μ wavelength and

$$N = N_D = 10^{25}/m^3 ;$$

$$1/g = \tau = 10^{-13} \text{ sec.}$$

$$m^* = 0.16\ m_o$$

$$\omega = 1.78 \times 10^{14} \quad \text{i.e.} \quad h\nu = .12 \text{ ev.}$$

Substituting these values in equations (61) and (62) the solutions are:

$$n = 3.1$$

$$k = .057$$

$\therefore$ the above absorption attenuation constant

$$\alpha = \frac{4\pi k}{\lambda} = .067\mu m^{-1}$$

The reflection coefficient is given by [34] .

$$R = \frac{(n-1)^2 + k^2}{(n+1)^2 + k^2} \qquad \text{i.e.}$$

$$R = 27\% .$$

2) For radiation of 300μ wavelength and

$$N = N_D = 10^{25}/m^3 \ ;$$
$$1/g = \tau = 10^{-13} \text{ sec.}$$
$$m^* = 0.16 \ m_o$$
$$\omega = 6.3 \times 10^{12} \quad \text{i.e.} \quad h\nu = .004 \text{ ev.}$$

Substituting into equations (61) and (62), we get that

$$n = 29.6$$
$$k = 53.7$$

$\therefore$ the above absorption attenuation constant

$$\alpha = \frac{4\pi k}{\lambda} = 2.2 \ \mu m^{-1} \ .$$

The reflection coefficient is given by

$$R = \frac{(n-1)^2 + k^2}{(n+1)^2 + k^2} = 97.5\% \ .$$

Absorbtion Constant Frequency Dependence

The solutions of equations (61) and (62) can be generalized for the two cases as follows:

1) The condition when $\omega^2 > g^2$ and $\frac{\beta}{\omega^2 + g^2} < n_c^2$

$$\text{where } \beta = \frac{Ne^2}{m^* \epsilon_o}$$

then

$$n^2 = n_c^2$$

$$k = \frac{g\beta}{2 n_c \omega^3}$$

$$\alpha = \frac{g\beta}{c\, n_c\, \omega^2}$$

where c is the velocity of light.

In this case the absorption constant is inversely proportional to the square of the incident radiation frequency.

2) The condition when $\omega^2 < g^2$ and $\frac{\beta}{\omega^2 + g^2} > n_c^2$

then

$$n^2 = \frac{\beta}{2g\omega}$$

$$k = \left(\frac{\beta}{2g\omega} \right)^{1/2}$$

$$\alpha = \frac{1}{c} \left(\frac{2\beta\omega}{g} \right)^{1/2}$$

This expression is the reciprocal of the "skin depth" of metals found in microwave studies [35] .

Thus, the variation of the absorption constant α with frequency is summarized in Figure 39 .

APPENDIX II

Recombination Processes

In section V, 3.2, it was assumed that the elctrons were excited to an impurity energy level Et of total concentration N_t, by the laser radiation. An equivalent statement is that excess holes are generated in the valence band by being excited from the impurity levels as in the figure below.

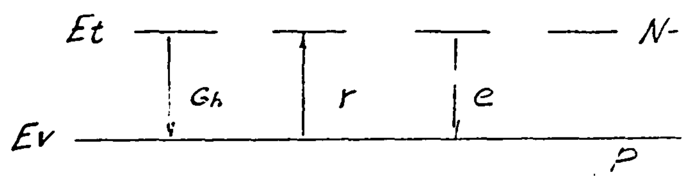

Figure 40 Recombination Model

To calculate the lifetime of a hole in the valence band, a rate equation similar to those used by Moll [29], is written:

$$\frac{dp}{dt} = -v_t \sigma_p{}^* N_t{}^* p + v_t \sigma_p{}^* (N_t - N_t{}^*) p_1 \qquad (63)$$

where

p is the number of holes in the valence band,

N_t* is the number of impurity states that have lost a hole by emission or excitation,

σ_p* is the capture cross-section for holes by states N_t*

v_t is the thermal velocity of holes,

$p_1 = N_v\, e^{-(Et - Ev)/k_BT}$, the number of holes in the valence band if the fermi-level was situated at Et.

The first term on the right-hand side of equation (63) denotes the recombination process r, and the second the thermal emission e of the holes from the impurity states.

Now

$$p = p_o + \Delta p$$
$$Nt^* = Nt_o^* + \Delta Nt^*$$

where p_o, Nt_o^* are the thermal equilibrium values.

Δp , ΔNt^* are the corresponding changes in the above values due to G_h, the generation rate resulting from the incident radiation. From

From charge neutrality conditions,

$$\Delta Nt^* = \Delta p \;.$$

Rewriting equation (63) in terms of the incremental changes Δp , ΔNt^*, and combining terms:

$$\frac{d\,\Delta p}{dt} = - v_t\, \sigma_p^*\, (Nt_o^* + p_o - p_1)\, \Delta p$$

Then the hole lifetime is defined as,

$$\tau = \Delta p \Big/ \frac{-d(\Delta p)}{dt} = \frac{1}{[\, v_t\, \sigma_p^*\;\; Nt_o^* + p_o - p_1 \,]} \qquad (64)$$

But $p_o = N_A \gg Nt_o^*$ and p_1 .

$$\therefore \qquad \tau \simeq \frac{1}{v_t\, \sigma_p^*\, N_A} \qquad (65)$$

Thus, for the magnitude of τ to be of the order of 10^{-4} sec. (refer section V, 2.2) with $N_A = 10^{19}$/cc. and $v_t = 10^7$ cm./sec.,

$$\sigma_p^* \approx 10^{-22} \text{ cm.}^2$$

From the literature [36], it is found that c_p is normally much larger in magnitude and only doubly positively charged donor states will provide such a small capture cross-section for holes.

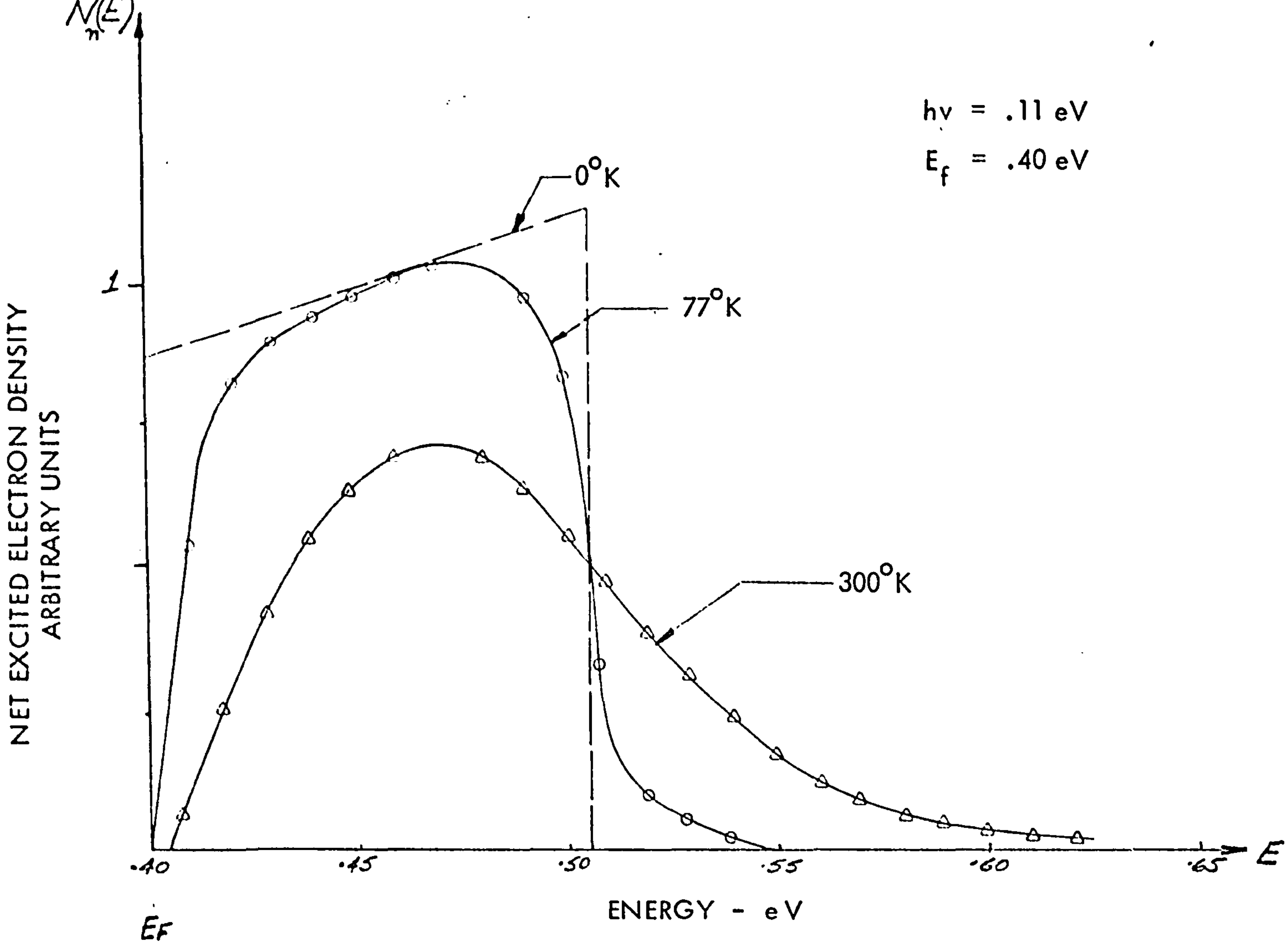

FIGURE 41(a). EXCITED ELECTRON ENERGY DISTRIBUTION.

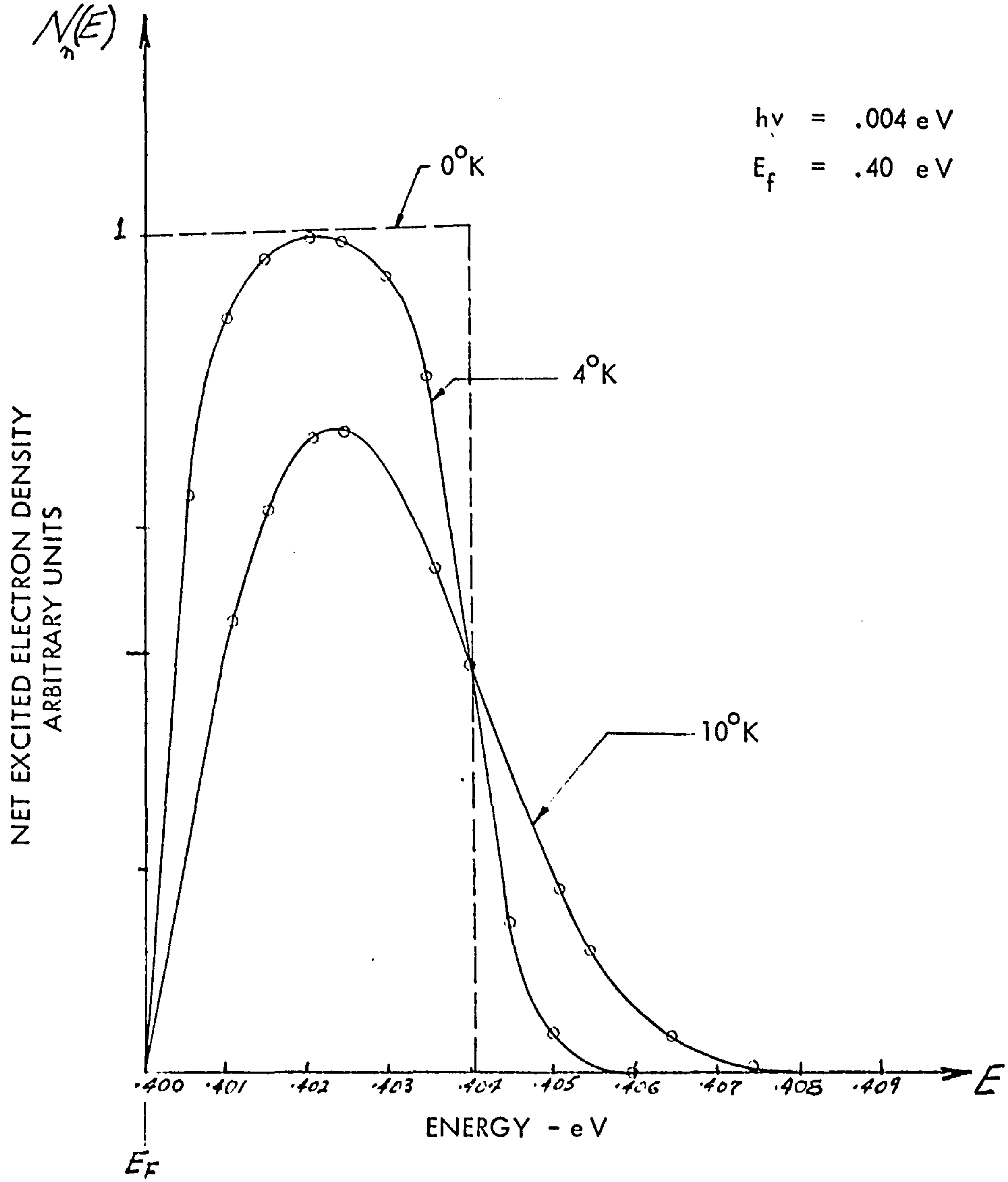

FIGURE 41(b). EXCITED ELECTRON ENERGY DISTRIBUTION.

REFERENCES

[1] C.A. Burnus and W. Gordy, "Submillimeter wave spectroscopy", Phys. Rev., Vol. 93, pp. 897-898, February, 1954.

[2] Meredith and F.L. Warner, "Superheterodyne Radiometers for Use at 70Gc/s and 140Gc/s", presented at IRE Orlando Millimeter and Submillimeter Conf., Orlando, Fla., January, 1963.

[3] R.A. Smith, F.E. Jones and R.P. Chasmar, "Detection and Measurement of Infra-Red Radiation", Clarendon Press, Oxford, England, Ch. III, 1957.

[4] W.S. Boyle and K.F. Rodgers, "Performance Characteristics of a New Low-Temperature Bolometer", J. Opt. Soc. Am., Vol. 49, pp.66-69, January, 1959.

[5] Y. Oka, K. Nagasaka and S. Narita, "Far-Infrared Germanium Detectors", Jap. J. of App. Physics, Vol. 7, No. 6, pp. 611-618, June, 1968.

[6] M.J.E. Golay, "A Pneumatic Infra-red Detector", Rev. Sci. Instr., Vol. 18, pp.357-362, May, 1947.

[7] J.R. Alday, "Millimeter Wave Detectors Using Pyroelectric Effect", IEEE Trans. on Electron Devices, Vol. 16, p.598, June 1969.

[8] E.H. Putley, "The Detection of Sub-mm Radiation", Proc. IEEE, pp.1412-22, November 1963.

[9] W.V. Houston, Phys. Rev., Vol. 57, p.184, 1940.

[10] J. Shewchun, A. Waxman and G. Warfield, "Tunneling in MIS Structures-I", Solid State Electronics, Vol. 10, pp.1165-1186, 1967.

[11] L. Esaki, Phys. Rev., Vol. 109, p.603, 1958.

[12] S. Green and P.D. Coleman, "The MOM Electric Tunneling Detector", presented at PIB Symposium on Submillimeter Waves, New York, N.Y., April 1970.

[13] W.E. Dahlke and S.M. Sze, "Tunneling in Metal-Oxide-Silicon Structures", Solid State Electronics, Vol. 10, pp. 865-873, 1967.

[14] R.M. Minton and R. Glicksman, "Theoretical and Experimental Analysis of Germanium Tunnel Diode Characteristics", Solid State Electronics, Vol. 7, pp.491-500, 1964.

[15] B.E. Deal and E.H. Snow, "Barrier Energies in Metal-Silicon Dioxide-Silicon Structures", J. Phys. Chem. Solids, Vol. 27, pp.1873-1879, 1966.

[16] A.S. Grove, "Physics and Technology of Semiconductor Devices", John Wiley and Sons, Inc., New York, Chap.9, 1967.

[17] W.P. Dumke, "Quantum Theory of Free Carrier Absorption", Phys. Rev., Vol. 124, no. 6, pp.1813-17, December 15, 1961.

[18] E.O. Kane, "Theory of Tunneling", J. App. Phys., Vol. 32, No. 1, pp. 83-91, January 1961.

[19] E.O. Kane, "Zener Tunneling in Semiconductors", J. Phys. Chem. Solids, Vol. 12, p.181-188, 1959.

[20] A.F. Gibbon, J.W. Granville and E.G.S. Paige, J. Phys. Chem. Sob Solids, Vol. 19, pp. 198-217, 1961.

[21] W. Franz, "Duration of the Tunneling Single Process", Phys. Stat. Solid., Vol.22, p.K139, 1967.

[22] M.A. Lee, B. Easter, H.A. Bell, "Tunnel Diodes", Chapman and Hall Ltd., London, Great Britain, 1967.

[23] A. Smith, J. Janak, R.B. Adler, "Electronic Conduction in Solids", McGraw Hill, Inc., 1967.

[24] D. Meyerhofer, G. Brown, H.S. Sommers, Jr., "Degenerate Germanium I;Tunnel, Excess, and Thermal Current in Tunnel Diodes", Phys. Rev., Vol. 126, no. 4., pp.1325-1341, May 15, 1962.

[25] C.T. Sak, R.N. Noyce, W. Schockley, Proc. Inst. Radio Engrs., Vol. 45, p. 1228, 1957.

[26] W. Shockley and R. Henley, Bull. Am. Phys. Soc., Vol. 6, p.106, 1961.

[27] P. Gray, D. De Witt, A.R. Boothroyd, "Physical Electronics and Circuit Model of Transistors", John Wiley and Sons, 1964.

[28] R.N. Hall, "Tunnel Diodes", IRE Trans. on Electron Devices", January 1960.

[29] J.L. Moll, "Physics of Semiconductors", McGraw-Hill Inc., Chap. 6, 1964.

[30] H.J.G. Meyer, "Infra-red Absorbtion by Conduction Electrons in Germanium", Phys. Rev.,Vol. 112, pp.298, No. 2, October 1958.

[31] R. Rosenberg and M. Lax, "Free-Carrier Absorption in n-Type Ge", Phys. Rev., Vol. 112, no.3, p.843, November 1958.

[32] Fan, Spitzer, and Collins, Phys. Rev.,Vol. 101, p.566, 1956.

[33] P. Drude, Phys. Z., Vol. 1, p.161, 1900.

[34] T.S. Moss, "Optical Properties of Semi-Conductors", Butterworths Publications Ltd., Chap. 3, 1959.

[35] S. Ramo, J. Whinnery, T. Van Duzer, "Fields and Waves in Communication Electronics", John Wiley and Sons Inc., Chap.4, 1965.

[36] A. Rose, "Concepts in Photoconductivity and Allied Problems", John Wiley and Sons, Chap. 7, 1963.

[37] Many, Goldstein, Grover, "Semiconductor Surfaces", North-Holland Publishing Co., Amsterdam, 1965.

[38] Holonyak, et al, Phys. Rev. Letters, Vol. 3, p. 167, 1959.

[39] Day, Gaddy, and Iversen "Detection of Fast Infrared Laser Pulses with Thin Thermocouples", Appl.Phys.Letters, Vol. 13, No. 9, pp. 289-290, November 1968.

[40] Contreras and Gaddy, "Nanosecond Response Time Room-Temperature Infrared Detection with Thin-Film Bolometers", App. Phys. Letters, Vol. 17, No. 10, pp. 450-453, November 1970.

[41] Gibson, Kimmitt and Walker, "Photon Drag in Germanium", App. Phys. Letters, Vol. 17, No. 2, pp.75-77, July 1970.

[42] Daneshevsky et al, "Dragging of Free Carriers by Photons in Direct Interband Transistions in Semiconductors", JETP, Vol. 31, No. 2, pp. 292-295, August 1970.

[43] J.S. Brugler, "Optoelectronic Nomenclature of Solid-State Radiation Detectors and Emiters", IEEE, J. Solid State Circuits, Vol. 5, No. 5, October 1970.